

# Type II and anomalous Cepheids in the *Kepler K2* mission

Monika I. Jurkovic<sup>1</sup>★, Emese Plachy<sup>2,3,4,5</sup>†, László Molnár<sup>2,3,4,5</sup>,  
Martin A. T. Groenewegen<sup>6</sup>, Attila Bódi<sup>2,3,4</sup>, Pawel Moskalik<sup>7</sup> and Róbert Szabó<sup>2,3,4,5</sup>

<sup>1</sup>*Astronomical Observatory of Belgrade, Volgina 7., 11060 Belgrade, Serbia*

<sup>2</sup>*Konkoly Observatory, Research Centre for Astronomy and Earth Sciences, Eötvös Loránd Research Network (ELKH), Konkoly Thege Miklós út 15-17, H-1121 Budapest, Hungary*

<sup>3</sup>*CSFK, MTA Centre of Excellence, Konkoly Thege Miklós út 15-17, H-1121 Budapest, Hungary*

<sup>4</sup>*MTA CSFK Lendület Near-Field Cosmology Research Group*

<sup>5</sup>*ELTE Eötvös Loránd University, Institute of Physics, Pázmány Péter sétány 1/A, H-1117 Budapest, Hungary*

<sup>6</sup>*Royal Observatory of Belgium, Ringlaan / Avenue Circulaire 3, 1180 Brussels, Belgium*

<sup>7</sup>*Nicolaus Copernicus Astronomical Centre of the Polish Academy of Sciences, ul. Bartycka 18, 00-716 Warszawa, Poland*

Accepted XXX. Received YYY; in original form ZZZ

## ABSTRACT

We present the results of the analysis of Type II and anomalous Cepheids using the data from the *Kepler K2* mission. The precise light curves of these pulsating variable stars are the key to study the details of their pulsation, such as the period-doubling effect or the presence of additional modes. We applied the Automated Extended Aperture Photometry (autoEAP) to obtain the light curves of the targeted variable stars which were observed. The light curves were Fourier analyzed. We investigated twelve stars observed by the K2 mission, seven Type II and five anomalous Cepheids. Among the Type II Cepheids EPIC 210622262 shows period-doubling, and four stars have modulation present in their light curves which are different from the period-doubling effect. We calculated the high-order Fourier parameters for the short-period Cepheids. We also determined physical parameters by fitting model atmospheres to the spectral energy distributions. The determined distances using the parallaxes measured by the Gaia space telescope have limited precision below 16 mag for these types of pulsating stars, regardless if the inverse method is used or the statistical method to calculate the distances. The BaSTI evolutionary models were compared to the luminosities and effective temperatures. Most of the Type II Cepheids are modeled with low metallicity models, but for a few of them solar-like metallicity ([Fe/H]=0.06) model is required. The anomalous Cepheids are compared to low-metallicity single stellar models. We do not see signs of binarity among our sample stars.

**Key words:** stars: variables: Cepheids – stars: oscillations (including pulsations)

## 1 INTRODUCTION

Type II Cepheids (T2Cs) are low mass ( $0.5 M_{\odot}$ ), radially pulsating stars. They form three subgroups, which can be separated by their periods: BL Herculis (BLH, with periods  $1 < P < 5$  days), W Virginis, including peculiar W Virginis stars ((p)WVir, with periods  $5 < P < 20$  days, and the RV Tauri (RVT, with periods greater than 20 days). The limits in between the periods follow the OGLE (Optical Gravitational Lensing Experiment<sup>1</sup>) classification scheme, e.g. see catalog of the OGLE-IV variables toward the Galactic Centre (Soszyński et al. 2017a).

Anomalous Cepheids (ACs) are variable stars with masses up

to  $1.3 M_{\odot}$  (Groenewegen & Jurkovic 2017b), which can pulsate in the fundamental or first radial overtone modes. Their pulsation periods range from 0.3 to 2.4 days (Soszyński et al. 2008, 2015). Their origin can have two different scenarios - they are either a result of a metal-poor single stellar evolution or they are the end result of the binary evolution Fiorentino & Monelli (2012).

Both of these variable types occupy the instability strip (IS) of the Hertzsprung-Russell diagram (HRD) (Catelan & Smith 2015), and they overlap in the short period range, but they form separate period-luminosity relations (PL-relations), see for example Wielgórski et al. (2022); Bhardwaj et al. (2021); Das et al. (2021); Bhardwaj (2020); Ripepi et al. (2019); Groenewegen & Jurkovic (2017b); Bhardwaj et al. (2017); Soszyński et al. (2015); Matsunaga et al. (2011); Soszyński et al. (2008), and references within. In the article by Braga et al. (2020) it is stated that the PL-relations of T2Cs, together with the RR Lyrae (RRL, short period pulsating

★ E-mail: mojur@aob.rs

† E-mail: plachy.emese@csfk.org

<sup>1</sup> <http://ogle.astrouw.edu.pl/>

stars) variable stars, can also be used as extragalactic distance indicators as are classical Cepheids used. The old stellar populations, such as T2Cs, probe the galaxies in different stages of interstellar material enrichment and star formation, thus providing an insight into the timeline of the galactic evolution. ACs are mostly found in dwarf galaxies, and could be used as independent distance indicators as well. From the evolutionary point of view, these are two very different types of stars, arriving onto the IS in different ways. T2Cs are in a late stage of their evolution, as they have reached the horizontal branch (HB) and they continue their last crossing of the IS before they lose all their outer shell and become a white dwarf (see Braga et al. (2020) for details). ACs are core He-burning stars that have higher masses than T2Cs, so they are brighter, (see, e.g., Fiorentino et al. 2006).

The theoretical hydrodynamic models of Smolec & Moskalik (2012, 2014); Smolec (2016); Buchler & Moskalik (1992); Moskalik & Buchler (1993, 1990); Kovács & Buchler (1988) show that BLHs and WVir stars exhibit non-linear phenomena such as period-doubling (PD), but long-term, precise observations are required to detect these. Clear detection of PD in a BLH star was reported, for the first time, by Soszyński et al. (2011) and Smolec et al. (2012) in the case of OGLE-BLG-T2CEP-279.

Cycle-to-cycle changes in WVir stars were already known (see Percy (2007)), but one must be careful about interpreting the observed phenomena. In the case of W Virginis itself Henden (1980) published their results stating that the star shows cycle-to-cycle variation, but the reanalysis of Plachy et al. (2017) confirmed that the observed phenomenon is PD.

The analysis of 924 T2Cs in the Bulge of the Milky Way from OGLE-IV data sets was published by Smolec et al. (2018). The detailed and in-depth insight into the nature of the pulsation of these stars showed that T2Cs can exhibit radial double-mode pulsation (pulsating simultaneously in the fundamental and first overtone modes). Then Soszyński et al. (2019) found two candidates for T2Cs pulsating in the first overtone. The phenomenon of period doubling appears in WVir stars with periods longer than 15 days and it becomes common and sometimes irregular in the RVT regime, but it is less common among BLH stars. Periodic modulation of the pulsation has been detected in all subgroups of T2Cs.

The space-based photometry of T2Cs was very limited before the *K2* mission of the *Kepler* space telescope (Borucki et al. 2010; Borucki 2016). The Convection, Rotation and planetary Transits mission (*CoRoT*, Baglin et al. 2007), operational between 2006 and 2013, observed only one T2C, *CoRoT* 0659466327, in which Poretti et al. (2015) found no additional frequencies beside the fundamental period and its harmonics. The original *Kepler* field-of-view contained one T2C, the RVT star DF Cygni. Detailed analyses of its behavior were published by Bódi et al. (2016); Vega et al. (2017); Plachy et al. (2018); Manick et al. (2019), finding additional, long-term period change due to the presence of a binary companion and a circumstellar disk, as well as the presence of chaos in its pulsation. Manick et al. (2019) found that DF Cyg is most probably a post red giant branch (post-RGB) binary. Plachy et al. (2017) published the first results of two T2Cs from the *K2* mission, namely KT Sco and M80 V1, where they found PD in the latter star.

In the case of ACs (Stetson et al. 2014) already described a possible Blazhko modulated (longer period variation of the amplitude in the minimum and maximum position of the light curve resulting in a light curve shape change as well observed in RRL type variables) or multiple-mode anomalous Cepheid, V129, in the dwarf spheroidal galaxy Leo I. Jurkovic (2018) found Blazhko-like modulation in FY Virginis, a Milky Way AC. Plachy et al. (2019)

found four anomalous Cepheids among the RRL candidate stars in the *K2* sample. Among these stars two show signs of a Blazhko-effect, making this the first definite discovery of this phenomenon in anomalous Cepheids. Soszyński et al. (2020b) found the first AC, OGLE-GAL-ACEP-091, pulsating in multiple modes and Plachy et al. (2021a) showed that the AC star XZ Cet is not just pulsating in a first-overtone but also has a strong secondary mode.

In this paper we use data from the *Kepler* space telescope during its extended *K2* mission (Howell et al. 2014). We examine which of the above mentioned phenomena can be detected in the T2Cs and ACs in the observed *K2* Campaigns. Section 2 describes the data selection process. In Subsection 2.1, we give the description of the target selection, in Subsection 2.2, we describe how the photometry was performed. The Fourier analysis of the sampled stars is described in detail in Subsection 2.3, and the Fourier analysis is explained. In Subsubsections 2.4.1, 2.4.2 and 2.4.3 results of the Fourier analysis of individual stars is presented. In Section 3, we use the Spectral Energy Distribution method to derive the physical parameters of each star, and then use it to construct the Hertzsprung–Russell Diagram (see Subsection 3.2), the Color–Magnitude Diagram (see Subsection 3.3) and the Period–Radius relation (see Subsection 3.4). Section 4 deals with the distance determination issue. In particular in Subsection 4.1, we show the Period–Magnitude relations, while in Subsection 4.2, we discuss how distances derived from the *Gaia* space telescope should be treated with caution. Finally, Section 5 contains the summary of our results.

## 2 THE *KEPLER* - *K2* DATASET

### 2.1 Target selection

The *Kepler* space telescope observed thousands of pre-selected targets during each campaign of the *K2* mission<sup>2</sup> (Howell et al. 2014), including several Cepheids. The Cepheid targets we proposed are based on the available classification from the literature. Targets were selected from the General Catalogue of Variable Stars (GCVS<sup>3</sup>), the Catalina Sky Survey (CSS<sup>4</sup>) and the All Sky Automated Survey (ASAS<sup>5</sup>) databases (Samus’ et al. 2017; Drake et al. 2014; Pojman-ski 1997). Among the selected and observed targets only two T2Cs have been analysed in detail so far (Plachy et al. 2017).

We reviewed the remaining Cepheid targets searching for T2Cs and ACs among them. We excluded the Cepheids in high stellar density fields from our investigations, such as the Galactic Bulge, observed in Campaigns 9 and 11, and the IC 1613 dwarf galaxy observed in Campaign 8, as these stellar fields require dedicated photometric solutions that are beyond the scope of this paper.

We found seven T2Cs and five ACs in the observed Campaigns, as shown in Table 1, which we analysed in detail. The table shows the number of the campaign in which the star was observed, the *Kepler* identification number (EPIC ID), the positions of the stars (right ascension, RA, and declination, DEC), the pulsational period (P) in days that were available in the The International Variable Star Index (VSX<sup>6</sup>), the average *Kepler* magnitude of the light curve, the

<sup>2</sup> <https://archive.stsci.edu/missions-and-data/k2>, <https://keplergo.github.io/KeplerScienceWebsite/>

<sup>3</sup> <http://www.sai.msu.su/gcvs/gcvs/>

<sup>4</sup> <https://catalina.lpl.arizona.edu/>

<sup>5</sup> <http://www.astrouw.edu.pl/asas/?page=main>

<sup>6</sup> <https://www.aavso.org/vsx/>

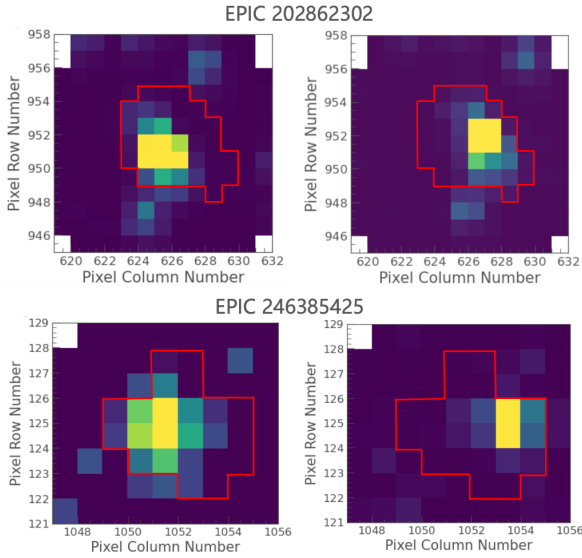


**Figure 1.** Examples of Target Pixel Frame (TPF) images for the stars EPIC 202862302 and EPIC 246385425 in extreme positions. The aperture pixel masks highlighted in red were determined by the autoEAP pipeline.

type of the variability determined in this work, and other known names from catalogs for the observed stars. Two long period T2C candidates, belonging to the RVT subgroup (see Table B1), were excluded from this study, since the length of the observed K2 data was insufficient for further investigation. We revealed that several former Cepheid candidates were wrongly classified, and they are listed in Table C1.

## 2.2 Photometry

The K2 mission has continued to deliver photometric data, but with lower quality compared to the original *Kepler* mission (after losing two reaction wheels that controlled the stability of the spacecraft). Systematic noise and instrumental signals resulted in light curves that needed to be cleaned from these artefacts. Additionally, the pointing deficiencies of the space craft created characteristic patterns in the data throughout each Campaign. All these additional signals could mimic real dynamical features of pulsating stars, such as amplitude modulation and cycle-to-cycle changes. Several pipelines have been developed to lessen or eliminate the instrumental issues. One of these has been optimized to separate the RR Lyrae type light variation with the highest possible quality, called the Extended Aperture Photometry (EAP, Plachy et al. 2019). In the EAP the algorithm chooses the pixels of the aperture by searching for the light variability of the target star at any time during the observation in them. That results in an extended aperture that covers the star at any position as it is demonstrated in Figure 1, where we display the pixel mask or a Target Pixel Frame (TPF) of the example stars at the extreme positions. Here we used the newest, automated version of EAP, the autoEAP pipeline (Plachy et al. 2021b; Bódi et al. 2021). The K2 Systematic Correction (K2SC, Aigrain et al. (2016)) was applied to further improve the quality of our light curves.

## 2.3 Analysis using Fourier decomposition

We performed the Fourier analysis with our own python code using the Lomb-Scargle (LS) method (Lomb 1976; Scargle 1982) to calculate the Fourier spectrum. We used the LS method as it is implemented in the *Astropy* package (Astropy Collaboration et al. 2013, 2018). The code first finds the frequency with the highest amplitude in the spectrum and after that does a consecutive pre-whitening with the integer multiples of that frequency. We used cosine-based Fourier series in the form of:

$$m(t) = m_0 + \sum_{i=1} A_i \cos(2\pi i f t + \varphi_i), \quad (1)$$

where  $m(t)$  is the calculated decomposition model,  $m_0$  is the average brightness in magnitude,  $A_i$  is the  $i$ th semi-amplitude,  $f$  is the frequency and  $\varphi_i$  is the phase of the given component.

The pre-whitening was performed until the frequency of the  $i$ th harmonic was lower than the average Nyquist limit:

$$f_{\text{Nyq}} = \frac{1}{2 < \Delta t >}, \quad (2)$$

where  $< \Delta t >$  is the average duration between consecutive observations, or the signal-to-noise ratio (S/N) of the given harmonic fell below 3 (Breger et al. 1993). After the iteration stopped all the amplitudes and phases, along with the mean magnitude and frequency, were fine-tuned by fitting all the Fourier components simultaneously to the light curve. This optimization process started from the previously determined values.

The errors of the Fourier components were estimated with a bootstrap method as follows. We re-sampled the light curves a hundred times by randomly selecting 60% of all measurements in each step. The free parameters were refitted to these subsets. The errors were calculated as the standard deviation of the distribution of the aggregated results of all the fits.

The relative Fourier parameters, that are widely used for the description of the light curves, defined by (Simon & Lee 1981; Simon 1986), are the ratio of the amplitudes of the main frequency and its harmonics:

$$R_{i1} = \frac{A_i}{A_1}, \quad (3)$$

and the relative phase differences:

$$\varphi_{i1} = \varphi_i - i\varphi_1, \quad (4)$$

where  $i = 2, 3$ .

## 2.4 Light curve features

The Fourier parameters of the K2 stars are listed in Table 2. The number of harmonics were derived with the detection limit of  $S/N \geq 3$  and the Nyquist frequency (24.468 c/d). These Fourier parameters were compared to those of the Cepheids measured by the OGLE Survey. We chose the Cepheid sample of the Large Magellanic Cloud (LMC), Soszyński et al. (2008); Udalski et al. (2015), where the clear Period-Luminosity relations validate the classification reliably. At the time of writing this paper the OGLE database provides Fourier parameters only in  $I$  photometric band. The  $V$  band parameters, however, are more suitable for comparison, since they are close to the  $K$  passband of the *Kepler* space telescope. We downloaded the available  $V$  band light curves and merged the data from OGLE-III and IV for the stars that were observed in both projects. Then

**Table 1.** The T2Cs and ACs examined in *K2* data. The first column gives the Campaign number in which the star was observed in the *K2* mission, while its EPIC catalog number is in the second column. The positions of the stars on the sky is given in the third and fourth columns (right ascension, RA, and declination, DEC) from the <sup>1</sup>(Gaia Collaboration 2020). The fifth column is the fundamental pulsation period (P) in days of the variable stars from the VSX database. The type of the variability - confirmed in this paper - is in the sixth column. The seventh column contains the other know names of the stars in the sample.

Camp.	EPIC ID	RA <sup>1</sup> [h m s]	Dec <sup>1</sup> [° ' "]	P <sub>VSX</sub> [days]	<Kp> [mag]	Type in this article	Other name
2	202862302	16 36 52.85	-28 05 34.21	1.956	12.926	AC	V1287 Sco
4	210622262	04 20 01.79	+17 16 45.83	16.635	16.882	WVir	CSS_J042001.7+171645
7	215881928	18 59 37.23	-23 21 52.28	1.835	14.606	BLH	V839 Sgr
7	217235287	19 16 10.99	-20 55 55.82	1.259	15.155	BLH	V527 Sgr
7	217693968	18 48 09.79	-20 07 35.61	16.206	13.289	WVir	V377 Sgr
7	217987553	19 06 26.94	-19 36 35.28	13.429	12.482	WVir	V1077 Sgr
7	218128117	19 34 34.67	-19 21 39.99	2.119	12.735	AC	ASAS J193435-1921.7
7	218642654	19 06 03.13	-18 25 41.65	13.775	12.166	WVir	V410 Sgr
12	246015642	23 39 54.14	-09 05 01.74	1.071	15.399	AC	CSS_J233954.1-090502
12	246333644	23 22 33.10	-02 23 40.08	1.287	17.792	AC	CSS_J232233.0-022339
12	246385425	23 15 26.53	-01 22 28.66	1.502	17.972	AC	CSS_J231526.5-012228
13	247445057	05 05 14.25	+21 45 48.91	13.943	12.355	WVir	VZ Tau

**Table 2.** The calculated Fourier parameters of the stars from the *K2* sample.

EPIC ID	$f_1$	$\sigma f_1$	P <sub>1</sub>	$\sigma P_1$	A <sub>1</sub>	$\sigma A_1$	Harmonics	
202862302	0.5113902	0.0000017	1.9554540	0.0000065	0.16840	0.00004	17	
210622262	0.0599405	0.0000125	16.6832109	0.0034791	0.48477	0.00073	4	
215881928	0.5448335	0.0000012	1.8354231	0.0000040	0.28267	0.00007	20	
217235287	0.7943928	0.0000010	1.2588231	0.0000016	0.33988	0.00005	30	
217693968	0.0615492	0.0000053	16.2471649	0.0013990	0.40777	0.00028	3	
217987553	0.0744979	0.0000059	13.4231972	0.0010631	0.41338	0.00038	3	
218128117	0.4718607	0.0000012	2.1192695	0.0000054	0.32199	0.00007	48	
218642654	0.0725999	0.0000033	13.7741237	0.0006261	0.37290	0.00021	3	
246015642	0.9337528	0.0000010	1.0709473	0.0000011	0.23580	0.00005	25	
246333644	0.7769263	0.0000020	1.2871234	0.0000033	0.39774	0.00028	25	
246385425	0.6657856	0.0000026	1.5019850	0.0000059	0.35242	0.00030	30	
247445057	0.0715535	0.0000054	13.9755568	0.0010547	0.45317	0.00044	3	
EPIC ID	R <sub>21</sub>	$\sigma R_{21}$	$\varphi_{21}$	$\sigma \varphi_{21}$	R <sub>31</sub>	$\sigma R_{31}$	$\varphi_{31}$	$\sigma \varphi_{31}$
202862302	0.3497	0.0002	4.5784	0.0632	0.1119	0.0003	2.8506	0.0951
210622262	0.1567	0.0017	6.1032	0.5019	0.0862	0.0017	3.5409	0.7547
215881928	0.2027	0.0003	5.1638	0.0539	0.123	0.0003	2.4219	0.0812
217235287	0.2247	0.0002	4.5201	0.0439	0.1543	0.0002	3.6138	0.0658
217693968	0.0574	0.0008	1.2767	0.2379	0.0819	0.0009	2.5225	0.3571
217987553	0.3849	0.0011	5.5215	0.2654	0.1000	0.0010	2.3702	0.3971
218128117	0.4513	0.0003	4.7151	0.0518	0.2095	0.0002	2.8334	0.0776
218642654	0.2382	0.0006	6.1255	0.1492	0.0999	0.0006	2.5737	0.2230
246015642	0.4450	0.0003	4.0950	0.0525	0.3264	0.0003	2.1435	0.0787
246333644	0.5081	0.0007	4.1728	0.1061	0.3552	0.0007	2.1509	0.1589
246385425	0.5264	0.0009	4.4309	0.1374	0.3355	0.0008	2.5007	0.2063
247445057	0.1554	0.0011	0.5144	0.2902	0.1207	0.0009	2.2681	0.4331

we excluded those stars that have less than fifty measurements altogether. For the rest, we calculated the Fourier coefficients with our python code mentioned above. The second harmonic peak turned out to be below our signal-to-noise threshold for a significant number of stars, which we then also excluded. For error estimation we chose a computationally less expensive method than the bootstrap. Errors were considered as square root of the variance from the diagonal of the covariance matrix, which was calculated by `scipy's curve_fit` method (Virtanen et al. 2020). The calculated *V* band Fourier parameters are provided in the Appendix A.

In Figure 2, we show the comparison of Fourier parameters for *K2* and OGLE stars, where the parameters are displayed as a function of the logarithm of the period in days. Colors and symbols indicate the different variability types, and we can check whether the *K2* stars are in the location where they should be according to their type. There are overlaps between the different groups, so the stars were checked individually in all four plots. Ideally, the position should clearly refer to a certain type at least on one of the plots. This is the case for the five WVir stars in the the  $\log P - \varphi_{21}$  plot, where they are clearly separated from the fundamental mode

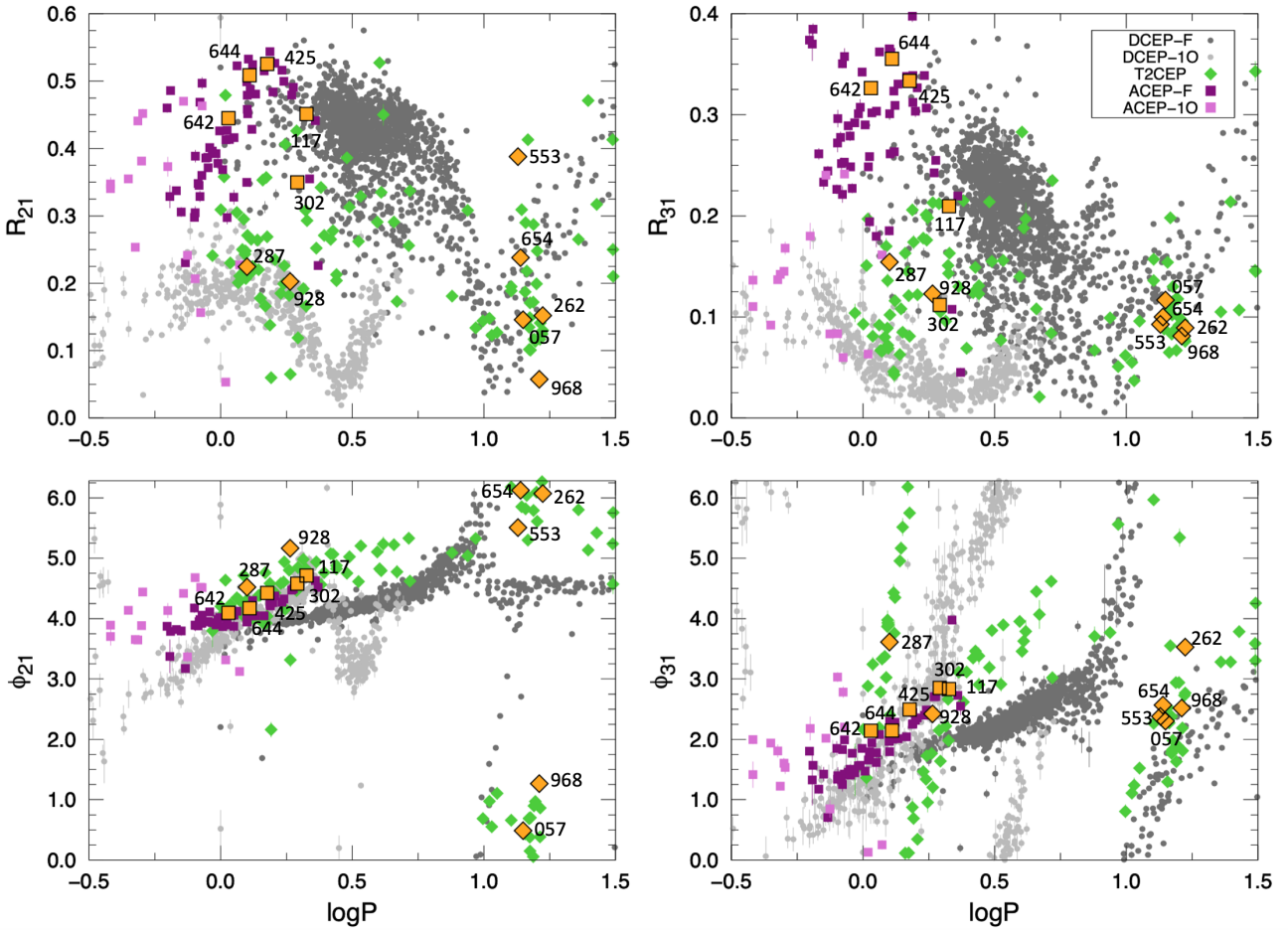


**Figure 2.** The cosine-based Fourier parameters ( $R_{21}$ ,  $R_{31}$ ,  $\phi_{21}$  and  $\phi_{31}$ ) versus the logarithm of the pulsational periods in days ( $P$ ) of the *K2* Cepheids (large orange symbols, and identified by the last three numbers of their EPIC identifier) plotted with the OGLE Large Magellanic Cloud Cepheids Fourier parameters from the *V* band data. Fundamental mode classical Cepheids (DCEP-F) are presented with dark grey points, first overtone classical Cepheids (DCEP-10) are in light grey points, Type II Cepheids (T2C) are green diamonds, fundamental mode anomalous Cepheids (AC-F) are shown in dark purple squares and first overtone anomalous Cepheids (AC-10) are presented with pink squares.

classical Cepheids (DCEP-F) with similar periods. The two BLH stars (marked as 287 and 928) are in the region of first overtone classical Cepheids (DCEP-10) in the  $\log P - R_{21}$  plane, but are distant from them in at least two other panels. We can be also confident in the type of the three shorter period ACs, but the two longer ones, EPIC 218128117 and EPIC 202862302, are not distinct from BLH stars in any panels. This shows that Fourier parameters have limitations when we try to use them for classification purposes of the ACs and T2Cs.

Investigating the Fourier parameters of higher orders, we may overcome the problem of precise classification. Therefore we calculated  $R_{i1}$  up to the highest possible  $i$  values for BLH and AC stars in our sample, and displayed the changes of these harmonic series in Figure 3 (both on linear and logarithmic scales). Unfortunately, no database for high-order Fourier parameters is available for comparison, but this can change with the massive analysis of Cepheids observed by the Transiting Exoplanet Survey (TESS) space telescope in the future. The first step has already been taken in the paper of Plachy et al. (2021a), where nine ACs and one BLH stars were analysed. Clearly, the decrease is not monotonic towards higher harmonic orders, and at some point(s)  $R_{i1}$  is higher than  $R_{(i+1)1}$ . The positions of these local minima (dips) vary from star

to star, and do not seem to correlate with the pulsation periods. The sequences of amplitude ratios were investigated in RRL stars too (Benkő et al. 2016), but there, a slight correlation was detected between the periods and the positions and depths of the dips.

#### 2.4.1 Anomalous Cepheids

In the sample we found five ACs: EPIC 202862302 from Campaign 2, EPIC 218128117 from Campaign 7, and EPIC 246015642, 246385425 and 246333644 from Campaign 12. Their phased light curves are shown in Figure 4 on the left panel with purple color. In the cases of EPIC 218128117 and 246385425 the decisive feature regarding classification is the bump on their descending branch, which is not present in any classical Cepheid (DCEP) with similar pulsation periods, and their positions in the Fourier parameter space (see Figure 2). The stars EPIC 246333644 and 246385425 are investigated in further detail, because they show some scatter in their light curves, but it was determined that the scatter is a consequence of the photon noise set by the light-gathering power of the telescope, and not a physical phenomena in the stars. We do not detect a Blazhko-like modulation in these stars.

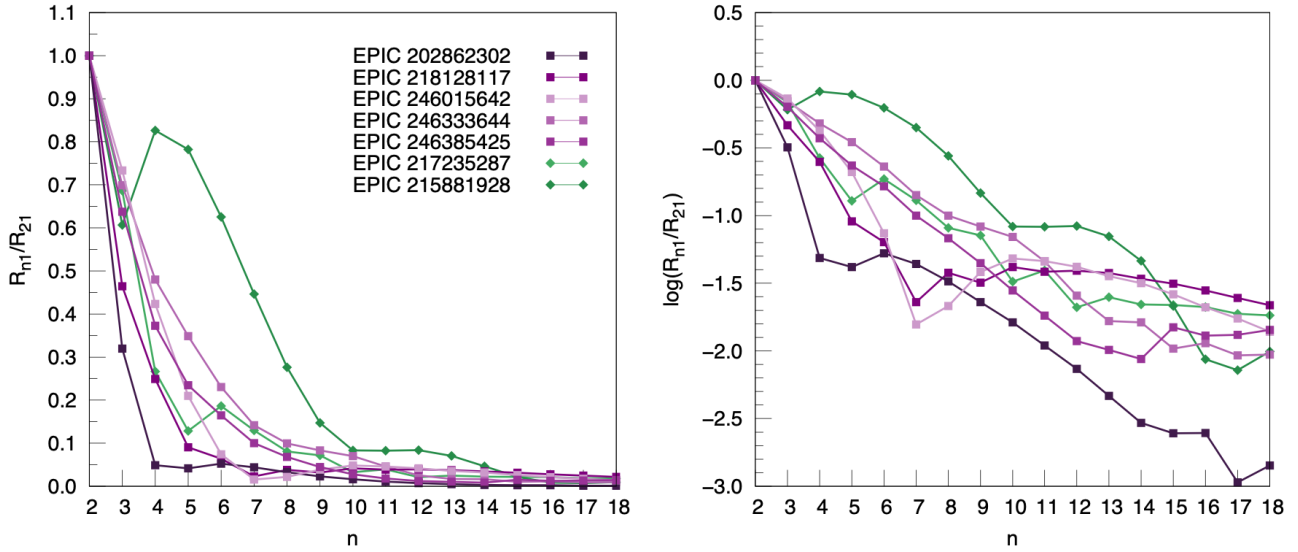


**Figure 3.** High-order Fourier relations of the amplitudes ( $\frac{R_{n1}}{R_{21}}$ ) for the ACs (purple) and the BLH stars (green) in the *K2* sample versus the number of detected harmonics. Values of the amplitudes ( $\frac{R_{n1}}{R_{21}}$ ) are normalized and displayed on linear (left) and logarithmic (right) scales.

In Figure 4, the right panel shows the Observed–Calculated (O–C) diagrams for the pulsation periods of the stars for the duration of the *K2* data set. The O–C values were computed from the maxima of the pulsation cycles with a template fitting method. These values show a low scatter in the range of a few minutes (the maximum is  $\sim 10$  minutes in EPIC 202862302). The pulsation amplitudes also vary within  $\sim 5$  mmag. At this low level we cannot decide whether these are instrumental or intrinsic variations, especially in the fainter stars where observational noise is significant (in the case of the star EPIC 46385425 it can reach 40 mmag).

Kovtyukh et al. (2018) noticed a presence of  $H_\alpha$  emission in the spectra of the star EPIC 202862302, which was classified as a T2C previously. The measured metallicity would be compatible with an AC ( $[Fe/H] = -1.94$  dex (see Tables 4 and 5), as they are described in Fiorentino & Monelli (2012). Our new classification combined with detection of  $H_\alpha$  emission by Kovtyukh et al. (2018) would make this the first known AC showing such a feature.

For the stars EPIC 218128117 and 246385425 the metallicity given in the literature (see Table 4 and 5) is from the *Gaia* DR2 (Gaia Collaboration et al. 2018), where these stars were identified as DCEPs. The metallicity was derived from the Fourier parameters of the *G*-band light curves. If these stars were DCEPs, then the transformation equation between the Fourier parameters and the  $[Fe/H]$  would be valid, but for ACs there is no known correlation (only few ACs have their metallicity measured from spectra). As a consequence, these metallicity data should be verified with direct spectroscopic measurements.

#### 2.4.2 BL Hercules stars

The BLH stars from the *K2* data sets are shown in Figure 4 with green color. The shapes of the light curves are very typical for the pulsation periods of these types. No period doubling or any other period or amplitude change is detectable in the *K2* light curves or in the O–C diagrams.

V839 Sgr or EPIC 215881928 in *K2* was proposed as an RRL

type variable, but the light curve shape and the period of its pulsation of 1.835 days confirm that it is a T2C, BLH subtype. In the *K2* mission, 43 pulsation cycles of V389 Sgr were observed. In Figure 4, we see the phase folded light curve in the left panel, the whole measured light curve in the middle panel and the O–C diagram in the right panel. Neither one of the panels show any period or amplitude change in the star EPIC 215881928.

V527 Sgr or EPIC 217235287 in *K2* was observed a few times in the past, by Kwee & Diethelm (1984), by the SuperWASP survey<sup>7</sup>, and by members of the American Association of Variable Star Observers (AAVSO<sup>8</sup>), for example. The International Variable Star Index (VSX<sup>9</sup>) database has a remark stating that this star changed its period since the first time it was observed by Uitterdijk (1935), who calculated it to be  $P = 1.258956$  days. The period measured from the *K2* light curve is 1.2588231 days (see Table 2). While this difference in the measured periods is detectable, and it can be traced to the first observations of this star, in the time span of the *K2* observational cycle EPIC 217235287 did not show any period change. The O–C diagram is flat, see Figure 4, right panel.

#### 2.4.3 W Virginis stars

The photometric precision and the high cadence are the key to reveal tiny instabilities in the pulsation. Period doubling and the seemingly irregular cycle-to-cycle changes are known phenomena in T2Cs. These phenomena are common in longer period variables, but rare at the short period end of the T2Cs (Catelan & Smith 2015).

The observed light curves of the five WVir stars in the *K2* observing cycles are shown in Figure 5 on the left panel, while the middle panel shows the phase folded light curves. The green color of the light curve changes with time, so when it is phase folded,

<sup>7</sup> <https://wasp.cerit-sc.cz/form>

<sup>8</sup> <https://www.aavso.org/>

<sup>9</sup> <https://www.aavso.org/vsx/>



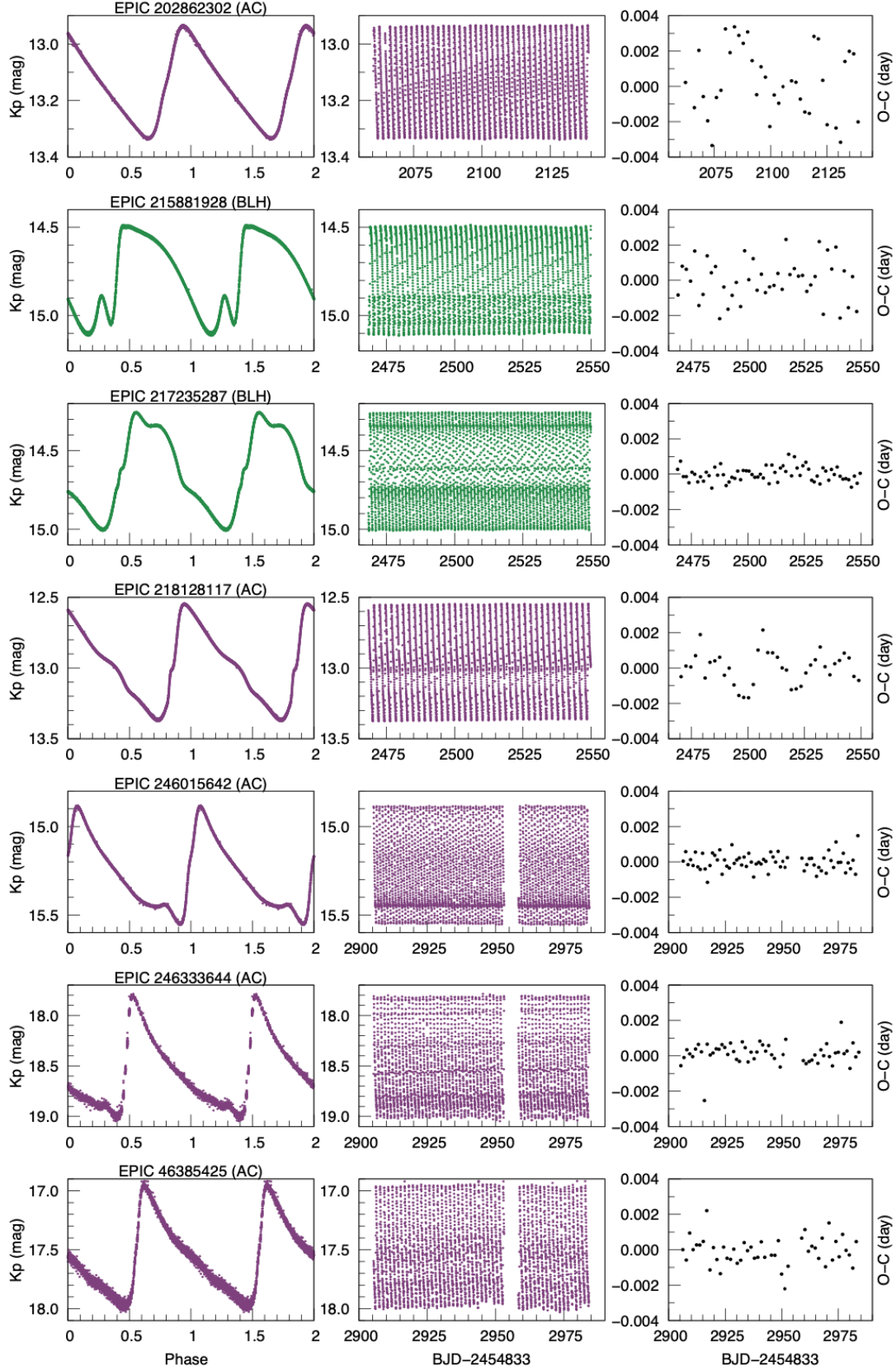


**Figure 4.** The phase folded light curves (left panel), observed light curves (middle panel) and O-C diagrams (right panel) of the ACs (purple) and BLHs (green) from the K2 data.

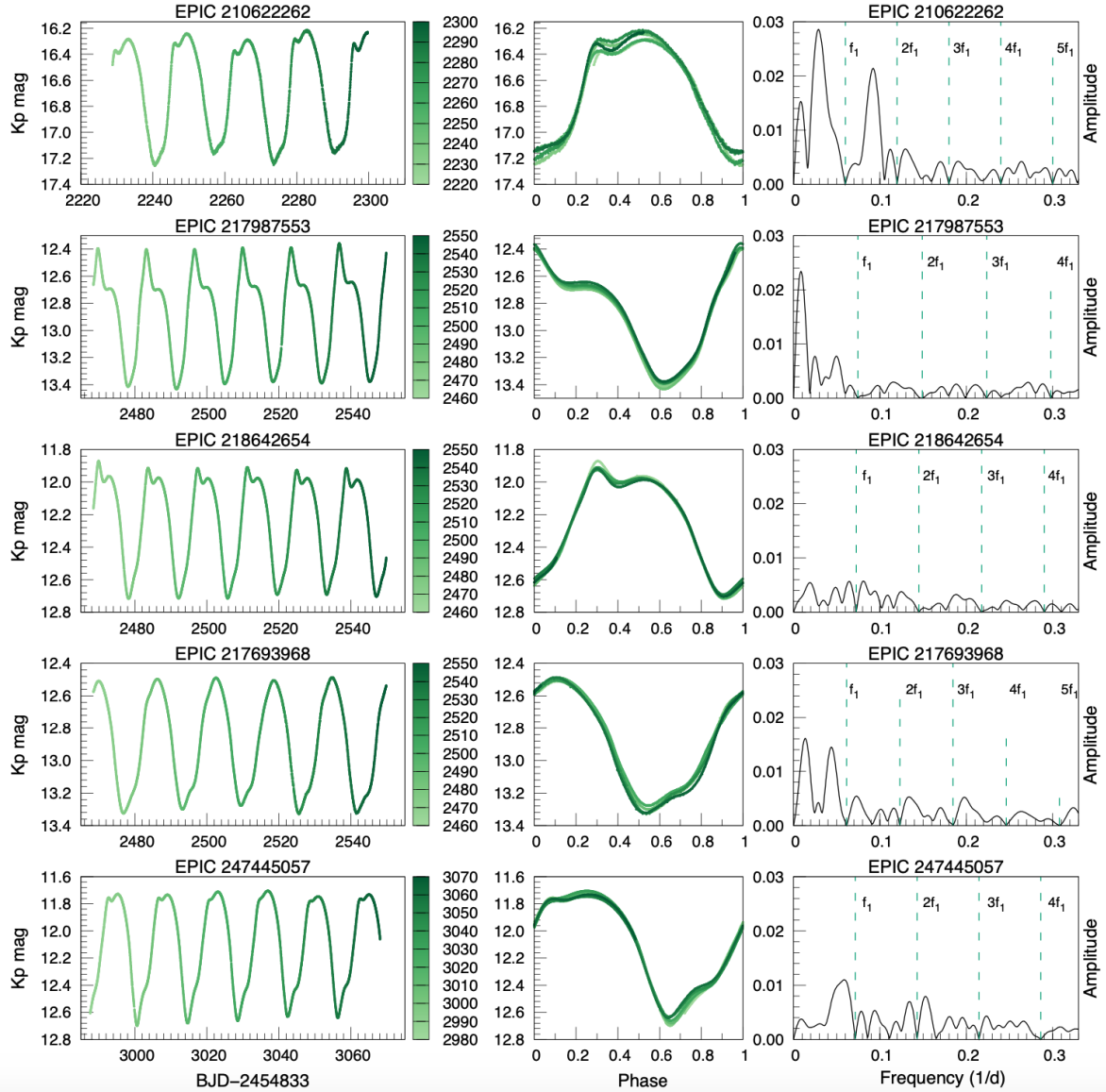


**Figure 5.** K2 light curves of WVir stars. On the left panel the total light curve is shown. The green scale goes from light green to dark green with time of the measurement (BJD-2454833) in days. The panel in the middle shows the phase folded light curves. The right hand panel shows the pre-whitened Fourier spectra (the frequency in [1/days] versus the amplitude in [mag]) of the light curves. The dashed green vertical lines show the position of the fundamental mode ( $f_1$ ) and the consequent harmonics ( $2f_1$ ,  $3f_1$ ,  $4f_1$  and  $5f_1$  in some cases).

the changes in the amplitude can be traced back to observational time. These light curves are studied in detail using the Fourier decomposition method. The Fourier spectra of these stars are shown in Figure 5 on the right panel. The residual Fourier spectra have the fundamental frequency ( $f_1$ ) and its harmonics ( $f_2 = 2f_1$ ,  $f_3 = 3f_1$ ,  $f_4 = 4f_1$  and  $f_5 = 5f_1$ ) up to the fourth order removed. The positions of the  $f_1$ ,  $f_2$ ,  $f_3$ ,  $f_4$  and  $f_5$  components are marked with vertical green dashed lines.

The O–C analysis was not applied to the WVir stars, since the total observed pulsation periods cover only a few cycles, so it would not give a meaningful result. In Figure 5 one can see that the WVir stars show cycle-to-cycle variation. The difference between the amplitudes of the consecutive cycles is in the range of a few mmag.

Only one star, EPIC 210622262 shows an alternation of the

even and odd cycles, the typical sign of period doubling (upper panels in Figure 5). The alternation is in the range of  $\sim 8$  mmag. Period doubling is also seen in the residual spectra in the form of a sub-harmonic peaks near  $0.5f_1$  and  $1.5f_1$ . We note that only four cycles are measured in the K2 mission for this star, but since period doubling is expected in WVir stars above  $P > 16$  days, it is very likely that we see this phenomenon here, as well. Due to the short time span of the measurement, the period-4 behaviour can not be confirmed ( $4 \times 16.6 = 66.6$  day, which is too close to the length of the observing run), but it is highly likely to be present in this star. After phasing the data with  $2 \times 16.6524$  day period, the minima and maxima seem to split into two values.

The star EPIC 247445057 (VZ Tau) was found to be a member of the open cluster Platais 4 by Zejda et al. (2012). Since VZ Tau is pulsating in a regular manner as a WVir type star, it would be worth



investigating if it is truly an open cluster member, since a WVir star should belong to an old population of stellar objects. In Figure 5, on the left panel, the light curve of this star shows changes in the shape of the maximum varying from one pulsation to the other. Again, this cannot be further investigated due to the shortness time span of the observations in each K2 observational cycle, but would be worth investigating further in detail.

### 3 PHYSICAL PARAMETERS

In this section, we explore different techniques that can tell us more about the physical parameters of the stars in our K2 sample. We calculate the effective temperatures and luminosities (see Subsection 3.1). The evolutionary status of the stars is examined in Subsection 3.2. We use data from the *Gaia* space observatory to plot the color-magnitude diagram (more in Subsection 3.3). In Subsection 3.4, we calculate the radii of the sample stars. We examine if any of these methods would be more suitable for the classification than the Fourier parameters derived from the light curves in combination with the light curve shapes.

#### 3.1 Spectral Energy Distribution

The physical parameters of individual stars were determined using the program `More of DUSTY`, MoD (Groenewegen 2012), an extension of the dust radiative transfer code DUSTY (Ivezic et al. 1999). For a given distance, reddening, and stellar model atmosphere the program determines the best-fitting luminosity by comparing the calculated spectral energy distribution (SED) to a set of observed magnitudes with errors. By testing different model atmospheres the best-fitting photometric effective temperature and luminosity is determined. For lower metallicities the calculated luminosities get larger. The effect is small: +3% for 1 dex in [Fe/H]. MARCS model atmospheres are used (Gustafsson et al. 2008), for  $\log g = 2.0$ , one solar mass, and solar metallicity. The effect of using non-solar metallicity models on the best-fitting luminosity is negligible compared to the errors in distance and reddening. None of the stars show evidence for any significant infrared excess and the dust optical depth is set to zero.

Distances are taken from Bailer-Jones et al. (2021) which are based on *Gaia* Early Data Release 3 (EDR3) data (Gaia Collaboration et al. 2021). For a detailed discussion on the precision of the distance determination see Section 4. The interstellar reddening is determined from the 3D reddening map of Green et al. (2019)<sup>10</sup> that is based on *Gaia* DR2, 2MASS, and Pan-STARRS 1 data. For EPIC246015642 this value is not available and the 3D reddening map of Lallement et al. (2018)<sup>11</sup> is used.

The data for the SED fit are collected from a plethora of sources. In the UV we used data from the Galaxy Evolution Explorer (GALEX, Bianchi et al. 2017). The visible and infrared parts of the spectra were covered with observations from *Gaia* EDR3 (the  $G$ ,  $G_{BP}$ , and  $G_{RP}$  magnitudes; Gaia Collaboration et al. 2021), the Tycho catalog (Høg et al. 2000), the 2MASS catalog (Skrutskie et al. 2006; Cutri et al. 2003), the DENIS catalog (Epchtein et al. 1999)<sup>12</sup>, the UKIDSS survey results (Lucas et al. 2008), the

Vista Hemisphere Survey (VHS; McMahon et al. 2013)<sup>13</sup>, and the ALLWISE catalog (Wright et al. 2010)<sup>14</sup>.

The resulting best fits are shown in Figure 6, and the parameters are summarised in Table 3. Columns 2, 3, 4, and 5 give the *Gaia* EDR3 source ID, parallax, Goodness of Fit (GoF), and Renormalised Unit Weight Error (RUWE). Three of the GoF values are large ( $>6$ ), but all RUWEs are smaller than 1.4 which is considered to be cutoff for problematic astrometric solutions (where a problematic astrometric solution could be an indicator of a binary system). Column 6 lists the distance from Bailer-Jones et al. (2021), and Column 7 is the interstellar reddening. The last two columns list the results from the fitting, namely the best fitting effective temperature and luminosity. The error in  $T_{\text{eff}}$  is about 125 K, while the error in the luminosity is the internal fitting error for the adopted distance.

#### 3.2 The Hertzsprung–Russell Diagram

The Hertzsprung–Russell Diagram (HRD) is constructed using the  $L$  and  $T_{\text{eff}}$  values for the stars we have examined (see Table 1). Figures 7 and 8 show the place of our program stars together with the T2Cs and ACs taken from Groenewegen & Jurkovic (2017a) for the Small Magellanic Cloud (SMC) and LMC. The evolutionary models are from the BaSTI (Bag of Stellar Tracks and Isochrones<sup>15</sup>) models (Hidalgo et al. 2018). The use models with solar-scaled heavy metal elements, with no diffusion, and no mass-loss.

The literature data for  $T_{\text{eff}}$ , the surface gravity ( $\log g$ ), and metallicity ([Fe/H]) are given in Table 4. From the seven T2Cs in our K2 sample, four have metallicity data available in the literature. Two of them, EPIC 217987553 and 217696968, have metallicities, [Fe/H]=−0.804 and −0.567, respectively, putting them in the slightly metal-poor category, while two more, EPIC 217235287 and 215881928, have metallicities of [Fe/H]=−0.042 and −0.058, making them stars with solar-like metallicities. These measurements motivated us to plot the BaSTI models with three different metallicities for T2Cs. In the case of the T2Cs the metallicities are [Fe/H]=−2.50, −1.55, and +0.06 dex. The horizontal branch (HB) models are shown with their masses ranging from  $0.47 M_{\odot}$  to  $0.80 M_{\odot}$ . The ACs in Table 4 have metallicities that range from [Fe/H]=−2.00 to −0.01 which is higher than what the models from Fiorentino et al. (2006) predict ( $Z=0.0001$  or [Fe/H]=−2.36), but are in good agreement with the models from Caputo et al. (2004) in which the metallicities of ACs are  $Z=0.0004$ . The most reliable metallicities come from direct spectroscopic measurements, and in Tables 4 and 5 these are [Fe/H]=−1.94 for EPIC 202862302 from Anders et al. (2019); and [Fe/H]=−1.513 and [Fe/H]=−2.00 for EPIC 218128117 and for EPIC 2460155642, respectively, from Hardegree-Ullman et al. (2020). The other metallicity and stellar parameter data are derived from photometry, astrometry, and other available data from catalogs, and the estimates made from them. The large differences in the metallicity data for each star could be the consequence of different methods used to determine the metallicities.

The models with the metallicities of −2.50 and −1.55 cover most of the T2Cs from the LMC and SMC, as well as the stars from our sample, EPIC 217235287, 217987553, 218642654, 247445057, and 217693968 shown in Figure 7. This is in agreement with the findings of Groenewegen & Jurkovic (2017a) and Bono et al. (2020).

<sup>10</sup> <http://argonaut.skymaps.info> the ‘Bayestar19’ dataset.

<sup>11</sup> <https://stilism.obspm.fr/>

<sup>12</sup> Vizier catalog B/denis/denis

<sup>13</sup> Vizier catalog II/359

<sup>14</sup> Vizier catalog II/328

<sup>15</sup> <http://basti-iac.oa-abruzzo.inaf.it/index.html>

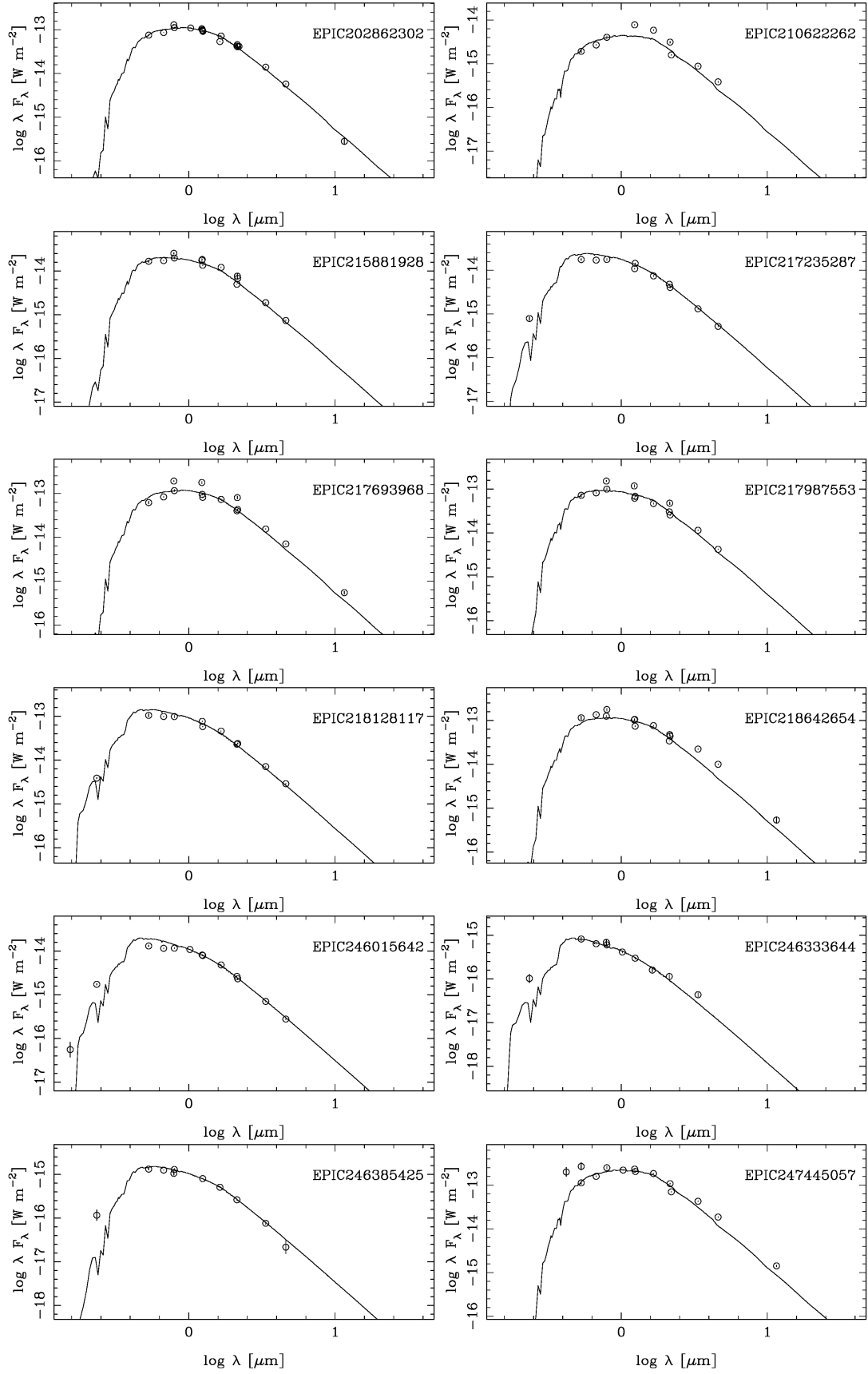


**Figure 6.** Model fits (the solid lines) to the observed photometry (points with error bars).

**Table 3.** Parameters from *Gaia* and results from the fitting.

EPIC	source ID ERD3	parallax (mas)	GoF	RUWE	Distance (pc)	$A_V$ (mag)	$T_{\text{eff}}$ (K)	$L$ ( $L_{\odot}$ )
T2Cs								
210622262	47299585774090112	$-0.1003 \pm 0.0780$	0.6217	1.027	7383 <sup>+2101</sup> <sub>-1728</sub>	1.24	5000	$19.33 \pm 1.99$
217235287	4082823506754098432	$0.0639 \pm 0.0329$	1.2925	1.064	8352 <sup>+2414</sup> <sub>-1505</sub>	0.43	6250	$92.83 \pm 3.70$
215881928	4075390224042082688	$0.1274 \pm 0.0269$	2.0615	1.102	6088 <sup>+1321</sup> <sub>-791</sub>	0.50	5625	$44.50 \pm 1.66$
217987553	4085507620804499328	$0.1495 \pm 0.0199$	0.8269	1.039	5297 <sup>+570</sup> <sub>-549</sub>	0.47	5250	$150.68 \pm 6.48$
218642654	4087335043492541696	$0.0505 \pm 0.0186$	7.9334	1.387	11574 <sup>+1806</sup> <sub>-1735</sub>	0.71	5500	$1085.55 \pm 86.12$
217693968	4085983537561699584	$0.1929 \pm 0.0194$	6.1186	1.289	4327 <sup>+452</sup> <sub>-359</sub>	1.15	5750	$191.96 \pm 11.51$
247445057	3415206707852656384	$0.2708 \pm 0.0225$	8.1617	1.376	3499 <sup>+236</sup> <sub>-252</sub>	1.15	5125	$214.78 \pm 11.49$
ACs								
202862302	6044434301761335808	$0.1830 \pm 0.0180$	0.32	1.013	4518 <sup>+323</sup> <sub>-431</sub>	1.18	5750	$200.66 \pm 5.86$
218128117	6869460685678439040	$0.0967 \pm 0.0201$	3.9358	1.198	7457 <sup>+1115</sup> <sub>-957</sub>	0.31	6500	$390.41 \pm 14.71$
246015642	2435741447518507392	$0.0453 \pm 0.0331$	3.4579	1.162	8353 <sup>+2643</sup> <sub>-1422</sub>	0.10	6500	$54.36 \pm 2.98$
246385425	2638680812622984960	$0.1101 \pm 0.0995$	-0.3849	0.980	4504 <sup>+1789</sup> <sub>-1098</sub>	0.16	6000	$1.36 \pm 0.03$
246333644	2637645489281432832	$-0.0774 \pm 0.1914$	0.9908	1.049	3722 <sup>+1664</sup> <sub>-1168</sub>	0.16	6750	$0.47 \pm 0.02$

In the case of EPIC 215881928 only the solar-like metallicity could reproduce its position on the HRD, which is in agreement with the metallicity from the literature ( $[\text{Fe}/\text{H}]=-0.058$ ). EPIC 210622262 is outside the limits of the evolutionary models, but the distance estimation, and thus the  $L$  and  $T_{\text{eff}}$  are uncertain, which could result in its current position on the HRD being inaccurate. EPIC 217693968 has a mass estimation from Huber et al. (2016) of  $M^c=0.963 M_{\odot}$ , but on all the evolutionary model figures (see Figure 7), only lower mass models, between 0.5 and 0.6  $M_{\odot}$ , cross the position of this star, making the previous mass estimation too high.

The star EPIC 210622262, which was identified as a WVir type star that is showing a PD effect in its light curve, is outside the  $-2.50$  and  $-1.55$  metallicity evolutionary tracks, but is close to the solar-like ( $+0.06$ ) metallicity model of 0.8  $M_{\odot}$  (together with some other stars from the Groenewegen & Jurkovic (2017a) sample). In Smolec (2016), the PD phenomenon is explained in detail for the T2Cs with masses from 0.6  $M_{\odot}$  up to 0.85  $M_{\odot}$ , however the metallicity of all the models is low. In this way, the models from Smolec (2016) do not give us an explanation of the PD phenomena in the solar-like metallicity star of 0.8  $M_{\odot}$ .

The ACs EPIC 216015642, 202862302, and 218128117 can be fitted well with the evolutionary models with metallicities of  $-1.55$  and  $-2.50$  as seen in Figure 8. In the case of EPIC 246333644 and 246385425 we see that they are outside the modeled HRD region. They are among the faintest stars in the sample, and due to the distance uncertainty their  $L$  was probably underestimated. The cases of EPIC 218128117 and 246385425 need further detailed investigation, since the available metallicity values in the literature (see Tables 4 and 5) are  $-0.01$  and  $0.12$ , respectively, which are too high for a typical AC. The problem with these data is that the *Gaia* DR2 estimates are based on their previous classification as DCEP stars, so the metallicity estimated from the Fourier parameters uses the correlation between the Fourier parameters and the metallicity for the DCEP stars. Gautschy & Saio (2017) shows different scenarios for binary channels to produce ACs, but non of their models cover the luminosity range of EPIC 246333644 and 246385425 either. If ACs would come from a binary channel evolution, they would have gone through a rapid mass-loss phase (Gautschy & Saio 2017), but

we do not see evidence of IR-excess in the SED around the observed ACs (see Figure 6).

For the AC EPIC 202862302 Kovtyukh et al. (2018) has measured a metallicity of  $[\text{Fe}/\text{H}]=-1.94$  dex. Looking at the evolutionary models of metal-poor stars from the BaSTI database two masses could be fitted on the position where EPIC 202862302 is on the HRD for the metallicity of  $[\text{Fe}/\text{H}]=-1.90$  dex: 1.5 and 1.8  $M_{\odot}$ , as it can seen in Figure 9.

### 3.3 Color-magnitude diagram from *Gaia* data

The color data measured by *Gaia* DR2 (in the blue filter (BP), red filter (RP) and the *Gaia* filter (G)) were collected from the *Gaia* database for the T2Cs and ACs in our K2 and for the known T2Cs, ACs and DCEPs. The list of known T2Cs (green), fundamental mode ACs (purple), overtone mode ACs (pink) and DCEPs (grey) were adopted from the catalogue by Ripepi et al. (2019) and Soszyński et al. (2017b, 2020a). The absolute magnitudes were calculated using the distances from the Bailer-Jones et al. (2018). The interstellar dust was taken into account as it was detected by *Gaia*. Figure 10 shows two sets of CMDs. On the left side the apparent G magnitude goes down to the 20 mag, and on the right side till 16 mag. The error bars on the colors are large, and the main source of the error is the reddening, and dust map inaccuracies. For stars with apparent magnitudes above 13-14 mag Molnár et al. (2021) the CMD is reliable in distinguishing between fundamental mode and overtone pulsation within one type of pulsating stars, but it is not too good for determining variable star classes (RRL vs ACEP vs DCEP vs T2C).

At this point the ACs and the T2Cs do not separate clearly, so the CMD should be used with caution when separating these subtypes of variable stars.

### 3.4 The Period-Radius Relation

The radius of the stars was calculated using the period-radius relations given in Groenewegen & Jurkovic (2017b), namely:

**Table 4.** Effective temperatures ( $T_{\text{eff}}$ ), surface gravity ( $\log g$ ), metallicities ( $[\text{Fe}/\text{H}]$ ), masses ( $M_{\odot}$ ) and radii ( $R_{\odot}$ ) from the literature for the AC stars in the K2 sample. References: <sup>a</sup>Miller (2015); <sup>b</sup>Huber et al. (2016); <sup>c</sup>Stevens et al. (2017); <sup>d</sup>Gaia Collaboration et al. (2018); <sup>e</sup>Kovtyukh et al. (2018); <sup>f</sup>Luo et al. (2018); <sup>g</sup>Stassun et al. (2018); <sup>h</sup>Tonry et al. (2018); <sup>i</sup>Anders et al. (2019); <sup>j</sup>Bai et al. (2019); <sup>k</sup>Stassun et al. (2019); <sup>l</sup>Xiang et al. (2019); <sup>m</sup>Gaia Collaboration et al. (2021); <sup>n</sup>Hardegree-Ullman et al. (2020); <sup>o</sup>Lucey et al. (2020); <sup>p</sup>Bonifacio et al. (2021); <sup>q</sup>Buder et al. (2021); <sup>r</sup>Anders et al. (2022).

ID	$T_{\text{eff}}^{\text{literature}}$ [K]	$\log g$ [cm/s <sup>2</sup> ]	[Fe/H] [dex]	$M$ [ $M_{\odot}$ ]	$R$ [ $R_{\odot}$ ]
ACs					
202862302	5428 <sup>b</sup>	3.542	-0.343	0.963	2.933
	4892.30 <sup>+114.33</sup> <sub>-43.40</sub> <sup>d</sup>	-	-	-	-
	5950 <sup>e</sup>	2.20	-1.94	-	-
	5432.32 <sup>i</sup>	2.212	-1.17	2.528	-
	4961.94 <sup>r</sup>	1.997	-1.52	0.854	-
218128117	7158 <sup>b</sup>	4.195	-0.034	1.506	1.586
	6345.00 <sup>+463.25</sup> <sub>-325.69</sub> <sup>d</sup>	-	-0.01	-	-
	6345 <sup>h</sup>	-	-	-	-
	6304.08 <sup>i</sup>	2.665	-1.513	1.854	-
	6742 ± 291 <sup>j</sup>	-	-	-	-
					8.959 <sup>k</sup>
	7190 <sup>n</sup>	4.019	-0.362	38.272	9.969
246015642	6353 <sup>a</sup>	-	-0.872, -0.742	-	-
	6459.00 <sup>+211.00</sup> <sub>-277.33</sub> <sup>d</sup>	-	-	-	-
	6101.79 <sup>i</sup>	2.622	-2.00	0.794	-
	-	-	-	1.290 <sup>k,d</sup>	2.652
	7098 <sup>n</sup>	4.039	-0.162	2.902	2.689
	5966.6 <sup>p</sup>	3.36	-0.39, -0.76	-	-
246385425	6191 <sup>a</sup>	-	-0.579, -0.548	-	-
	-	-	0.12 <sup>+0.4</sup> <sub>-0.5</sub> <sup>d</sup>	-	-
	6346.22 <sup>i</sup>	4.366	-0.919	0.900	-
	6060.0 ± 285 <sup>k</sup>	4.846	-	1.130	0.664
	5790.3 <sup>p</sup>	4.610	-0.14, -0.15	-	-
	6208.41 <sup>r</sup>	4.238	-1.467	0.773	-
246333644	-	-	-	-	-

$$\log R(R_{\odot}) = 0.846 \pm 0.006 + 0.521 \pm 0.006 \log P(d), \quad (5)$$

for the T2Cs, and

$$\log R(R_{\odot}) = 0.972 \pm 0.005 + 0.692 \pm 0.034 \log P(d), \quad (6)$$

for the fundamental mode ACs.

We have also done a check of the radii by calculating it from the  $L$  and  $T_{\text{eff}}$  which were obtained from the SED fits using the Stefan-Boltzmann law:

$$L = 4\pi R^2 \sigma T_{\text{eff}}^4, \quad (7)$$

where  $L$  is the luminosity,  $R$  is the radius,  $\sigma = 5.6704 \times 10^{-8} \text{ W m}^{-2} \text{ K}^{-4}$  is the Stefan-Boltzmann constant, and  $T_{\text{eff}}$  is the effective temperature. All the resulting radii are given in Table 6, and shown in Figure 11.

The PR-relation and the calculated radii are not model independent, one should be sceptical about using them as a parameter for classification. The  $L$  calculated from the SED (given in Table 3) is significantly smaller than expected for an ACs, and thus this error

is transferred to the radius calculation, as it can be seen in the cases of EPIC 246385425 and 246333644.

#### 4 THE PERIOD-LUMINOSITY RELATION

The examined ACs and T2Cs form period-luminosity relations. In this section we test the limitation of the period-luminosity (magnitude) relations for the ACs and T2Cs (Subsection 4.1) and the measured distances (Subsection 4.2).

##### 4.1 The period-magnitude relations of the Type II and anomalous Cepheids

The period-magnitude (luminosity) relation of pulsating stars is a method that could help us determine in an independent way to which subgroup these stars belong to: the ACs or the T2Cs. We have taken the absolute *Gaia* magnitudes using the EDR3 data for the T2Cs, ACs and DCEPs classified in the Ripepi et al. (2019) article and plotted the period-magnitude relation without a correction for the dust (see Figure 12). In this general plot we can see that these three types of variables do not separate clearly, especially when the

**Table 5.** Same as Table 4, the T2C stars.

ID	$T_{\text{eff}}^{\text{literature}}$ [K]	$\log g$ [cm/s <sup>2</sup> ]	[Fe/H] [dex]	$M$ [M <sub>⊙</sub> ]	$R$ [R <sub>⊙</sub> ]
T2Cs					
210622262	5396 <sup>b</sup>	4.527	-0.237	0.868	0.841
	4349.70 <sup>+193.55</sup> <sub>-94.70</sub> <sup>d</sup>	-	-	-	-
	6955.06 <sup>f</sup>	-	-0.095	-	-
	5161.17 ± 6.72 <sup>l</sup>	1.512 ± 0.135	-1.222 ± 0.089	-	-
	5751 <sup>n</sup>	3.858	-0.290	2.926	3.344
217235287	5816 <sup>b</sup>	4.159	-0.042	1.025	1.366
	5882.00 <sup>+66.00</sup> <sub>-59.00</sub> <sup>d</sup>	-	-	-	-
	5616.18 <sup>i</sup>	2.526	-1.388	1.114	-
	-	-	-	-	7.554 <sup>k</sup>
	6150 <sup>n</sup>	4.062	-0.360	27.644	8.077
215881928	5966 <sup>b</sup>	4.222	-0.058	1.062	1.300
	5290.74 <sup>+74.26</sup> <sub>-261.74</sub> <sup>d</sup>	-	-	-	-
	5305.85 <sup>i</sup>	2.722	-0.621	1.531	-
	5724 <sup>n</sup>	3.621	-0.899	5.519	5.989
	5211.92 <sup>r</sup>	2.693	-0.679	1.121	-
217987553	5954 <sup>b</sup>	4.416	-0.804	-	-
	4985.00 <sup>+390.00</sup> <sub>-383.70</sub> <sup>d</sup>	-	-	-	-
	5475.06 <sup>i</sup>	2.451	-0.798	2.255	-
	-	-	-	-	30.529 <sup>k</sup>
	6029.06 <sup>r</sup>	4.013	-0.560	0.914	-
218642654	5265 <sup>b</sup>	2.902	-0.773	0.907	4.900
	4926.50 <sup>+117.87</sup> <sub>-149.5</sub> <sup>d</sup>	-	-	-	-
	4605 ± 114 <sup>j</sup>	-	-	-	-
	5252.0 ± 402 <sup>k</sup>	-	-	-	45.220
	4696.0 ± 99 <sup>o</sup>	2.63 ± 0.16	-	-	-
217693968	4951 <sup>b</sup>	2.606	-0.567	0.963	8.605
	4537.61 <sup>+313.39</sup> <sub>-106.61</sub> <sup>d</sup>	-	-	-	-
	-	-	-	-	28.134 <sup>k</sup>
	5492 <sup>n</sup>	2.749	-0.988	11.186	23.128
247445057	6867.91 <sup>c</sup>	-	-	-	-
	4211.00 <sup>+77.74</sup> <sub>-104.29</sub> <sup>d</sup>	-	-	-	-
	5419 ± 524 <sup>j</sup>	-	-	-	-
	4837.0 ± 282 <sup>k</sup>	-	-	-	19.578
	5000.0 <sup>m</sup>	-	-	-	-
	5325 <sup>n</sup>	2.457	-0.893	2.610	15.761
	5164.49 <sup>q</sup>	2.236	-0.327	-	-

apparent brightness of the examined stars is fainter than 16 mag (see the left panel in Figure 12).

#### 4.2 Parallax vs. distances

Calculation of the absolute magnitudes requires the use of either a PL relation or some direct distance measurement, such as geometric parallaxes. The *Gaia* mission is surveying the entire sky to collect astrometric and photometric data for nearly over a billion stars, and down to 20–21 magnitudes in the *G* band (Gaia Collaboration et al. 2016). We collected the parallaxes from the *Gaia* DR2 and EDR3

databases (Gaia Collaboration et al. 2018, 2021) and the geometric distances as derived from these data by Bailer-Jones et al. (2018, 2021). However, some of our target stars are quite faint, which affects how useful their parallaxes might be. Since *Gaia* is fundamentally a photometric mission, the accuracy of measuring stellar positions largely scales with brightness. Therefore the uncertainties in parallax are driven both by the brightness and distance of each target. Solutions fitted to position measurements with large fractional uncertainties could lead to highest-likelihood parallax values that are close to, or below zero. We can see this in the distribution of points from the Cepheid samples compiled by Ripepi et al. (2019) in Figure 13.



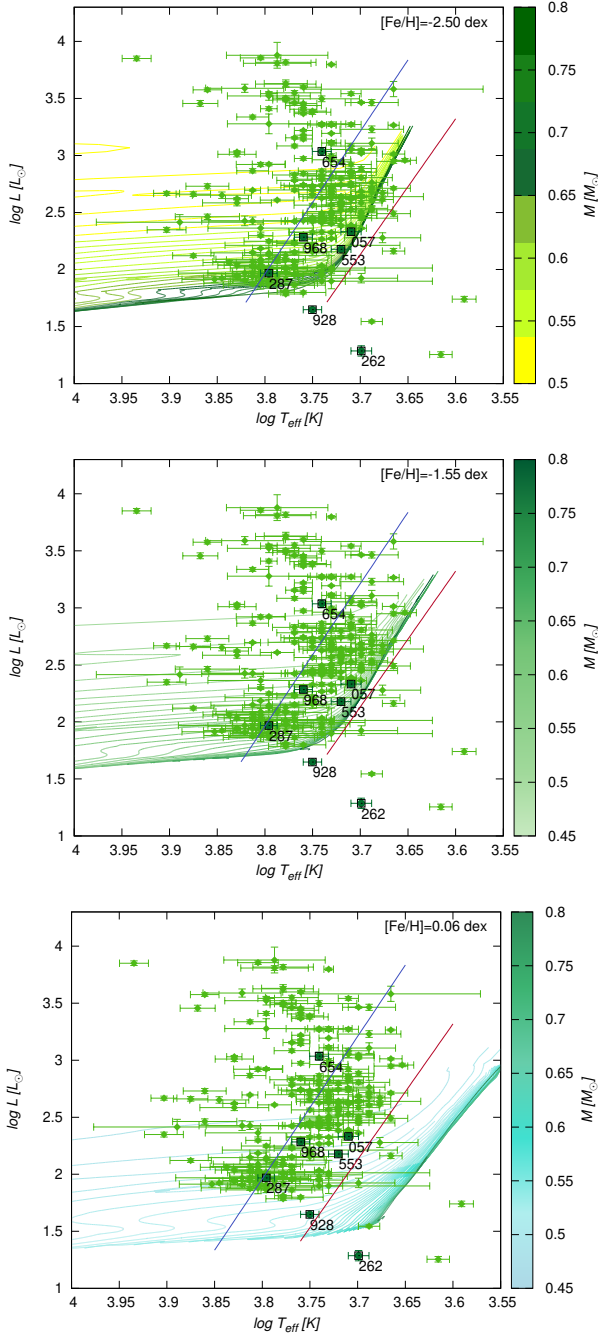


**Figure 7.** HRD: BaSTI models for low-mass stars evolving from the Horizontal Branch (HB) representing the T2C evolutionary tracks. Upper panel:  $[\text{Fe}/\text{H}] = -2.50$ , middle panel:  $[\text{Fe}/\text{H}] = -1.55$ , bottom panel:  $[\text{Fe}/\text{H}] = 0.06$ . The green crosses are T2Cs from the SMC and LMC taken from the Groenewegen & Jurkovic (2017a). The colored bars show the range of masses in solar masses from 0.45 to 0.8  $M_{\odot}$ .

As the *Gaia* parallaxes are statistical quantities based on a set of measurements, we need to be careful in interpreting them as inverse distances. In order to derive distance estimates, Bailer-Jones et al. (2018, 2021) uses a detailed, three-dimensional model of the Galaxy as a prior in their calculations. This has the benefit of limiting distances to the expected extent of the Milky Way. However, when there is not enough information in the parallax data (due to near-zero or negative values, and/or high fractional uncertainties),

**Table 6.** The calculated radii for the stars in the *K2* sample.

ID	$\log R^{\text{PRel.}}$ [ $R_{\odot}$ ]	$\log R^{\text{SED}}$ [ $R_{\odot}$ ]
T2Cs		
210622262	1.482	0.768
217235287	0.898	0.915
215881928	0.983	0.847
217987553	1.434	1.172
218642654	1.439	1.560
217693968	1.476	1.145
247445057	1.442	1.269
ACs		
202862302	1.258	1.155
218128117	1.198	1.193
246015642	0.993	0.765
246385425	1.094	(0.033)
246333644	1.048	(-0.300)

this method will assign distances close to the densest, and thus most preferred part of the prior. We can see this if we compare the calculated geometric distances to the measured parallaxes in Figure 13. Here we applied the necessary parallax zero-point correction to the measurements (Lindgren et al. 2021). The plots clearly show that stars that are both faint and have small or negative parallaxes, concentrate between 5–20 kpc. Those distances are dominated by the prior, and thus cannot be reliably used for our purposes.

If we now investigate the parallax and distance data for our target stars, we find that for the majority the two values agree with each other quite well. Only the three faintest targets are outliers. Out of those three, the anomalous Cepheid EPIC 246385425 appears to be in marginal agreement, while EPIC 210622262 and EPIC 246333644 have highly negative, and thus uninformative parallaxes. For those three stars absolute magnitudes cannot be reliably calculated from the *Gaia* data.

## 5 CONCLUSIONS

Using the *K2* data for the T2Cs and ACs we have performed our photometry with the autoEAP pipeline. Our final sample contained five ACs and seven T2Cs (two BLH and five WVir subtype stars). The classification was done using their Fourier parameters, which were compared to the *V* band OGLE data of the ACs, T2Cs and DCEP stars. We have used Fourier analysis to examine the pulsational properties of the sample stars. The ACs and T2Cs showed only pulsation in the fundamental mode. Their O–C diagrams did not indicate any period change during the duration of the *K2* Campaigns. None of the stars showed eclipses. In the O–C diagrams there was no evidence of binarity. The light curves did not show elliptical variability, which should be observed if the stars are in a close binary system. In the SED fits no IR-excess was observed, so there is no evidence of dust around the stars in the sample. The dust would be present in a close binary system exchanging material between the components. While the *Gaia* RUWE parameter is not a definite show of binarity, it confirms that there are no observed binary stars among the stars in our sample, neither T2Cs nor ACs.

The BLH and AC stars in our sample are stable, as seen in Figure 4, where we present their light curves, phase folded light curves and O–C diagrams. We note that we do not see indication of Blazhko-like amplitude or phase modulation. O–C values were

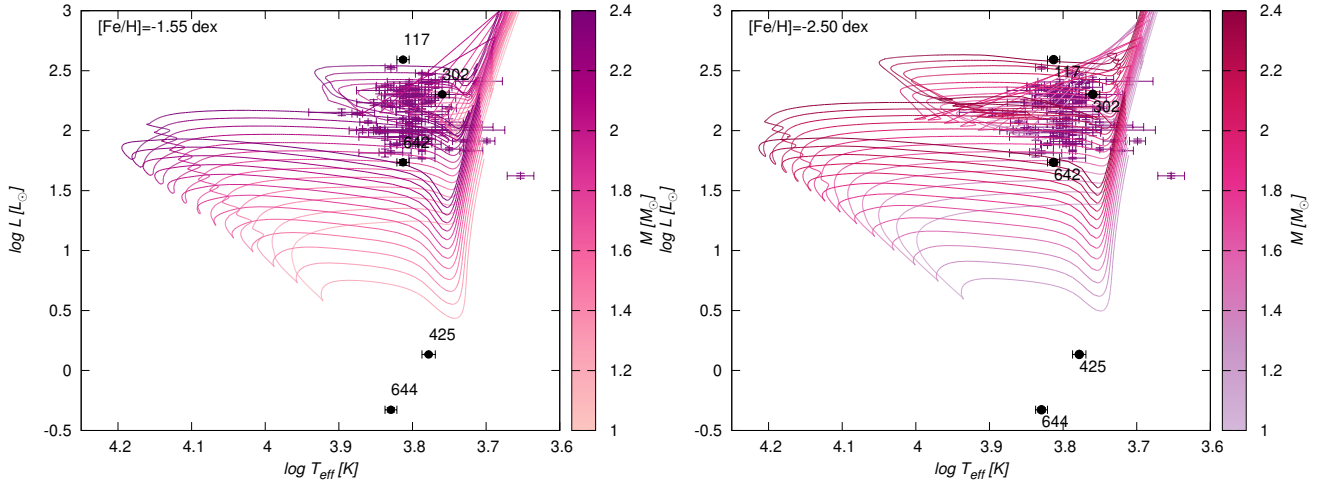


**Figure 8.** HRD: BaSTI models for single evolutionary models of ACs - on the left side  $[\text{Fe}/\text{H}] = -1.55$ , and on the right side  $[\text{Fe}/\text{H}] = -2.50$ . Stars 644 and 425 are ACs which are among the least bright ones, so their luminosity value is probably unreliable due to their parallax measurement error. The lilac crosses are ACs from the SMC and LMC taken from the Groenewegen & Jurkovic (2017a). The mass range, from  $2.4 M_{\odot}$  down to  $1.0 M_{\odot}$  with steps of  $0.1 M_{\odot}$ , is indicated by the change in the color bar shown on the right hand side of the plot.

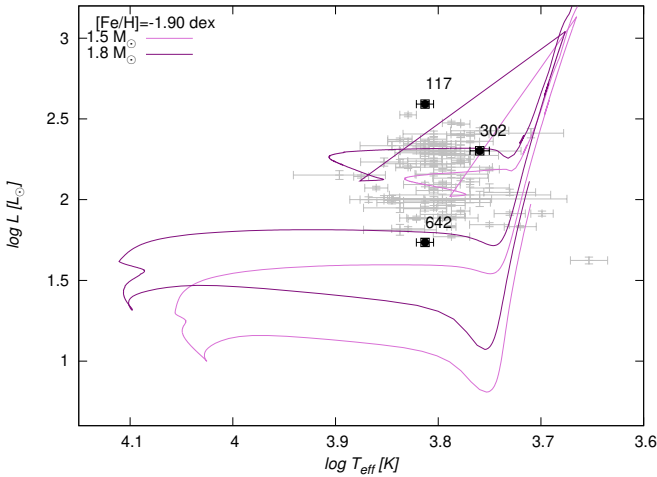


**Figure 9.** HRD: BaSTI models for single evolution of the AC EPIC 202862302. The purple line is a model of mass  $M = 1.8 M_{\odot}$  and the pink line is for mass  $M = 1.5 M_{\odot}$ . The metallicity of the model is  $[\text{Fe}/\text{H}] = -1.90$  dex, which is in good agreement of the measured metallicity of EPIC 202862302,  $[\text{Fe}/\text{H}] = -1.94$  dex. The grey crosses are ACs from the SMC and LMC taken from the Groenewegen & Jurkovic (2017a).

computed from the maxima of the pulsation cycles with a template fitting method. These values show a low scatter in the range of few minutes ( $\sim 10$  minutes at highest in EPIC 202862302). The pulsation amplitudes also vary within  $\sim 5$  mmag. At this low level we cannot decide whether these are instrumental or intrinsic, especially in the fainter stars where observational noise is significant (it can reach the 40 mmag at EPIC 246385425). Among WVir stars, EPIC 210622262 shows period-doubling, while the other WVir stars show cycle-to-cycle variation in their light curves.

We determined the luminosities, effective temperatures, and radii of the sample stars by modeling their SEDs with MoD. We used these parameters to place them on a HRD and analyze their

evolution using the BaSTI models. In the case of the ACs the models with  $[\text{Fe}/\text{H}]$  of  $-1.55$  and  $-2.50$  and masses from  $1.0 M_{\odot}$  to  $2.4 M_{\odot}$  fit the region occupied by the ACs. For the T2Cs, we used three models, two with metal-poor metallicities,  $[\text{Fe}/\text{H}] = -2.50$  and  $-1.20$  and one with metallicity close to solar,  $[\text{Fe}/\text{H}] = 0.06$ . The masses were from  $0.45$  to  $0.8 M_{\odot}$ . The solar-like metallicity models fit the blue edge of the instability strip of the observed T2Cs. The CMD for ACs, T2Cs, and DCEPs from the *Gaia* data does not clearly distinguish between these types of variables.

We show various ways that might be used to distinguish between T2Cs and ACs (and DCEPs, as well), making their classification unambiguous. Subsection 2.3 shows the Fourier parameters and the light curves. We have used the available astrometric and photometric data from the *Gaia* space telescope to construct the period–luminosity relation (Subsection 4) and the color–magnitude diagram (Subsection 3.3). Using the results from the SED fitting we constructed the HRD for all of our stars in the sample. We have plotted the period–radius (PR–relation) for our stars.

For the T2Cs and ACs the most reliable classification method is based on their Fourier parameters (as we show in subsection 2.3) and their light curve shapes. Despite the advances in data precision even the *Gaia* EDR3 data could not give a defining classification by plotting them on the color–magnitude diagram (see Subsection 3.3) where the T2C, ACs, DCEP-F and DCEP-IO overlap. The same is true for the PL–relation, see Section 4.

We have note that stars EPIC 246385425 and 246333644 are outliers. The cause for this is connected to their observed brightness. This led us to examine the limitation of the distances estimated from the *Gaia* space telescope. We confirm the findings from Plachy et al. (2021a) that for the pulsating stars that have a low apparent brightness the parallaxes are not good enough yet.

## ACKNOWLEDGEMENTS

This work has used *K2* targets selected and proposed by the RR Lyrae and Cepheid Working Group of the *Kepler* Asteroseismic Science Consortium (proposal numbers C4: GO4066, C7: GO7014, C10: GO10041, C12: GO12070, C13: GO13070). Funding for the

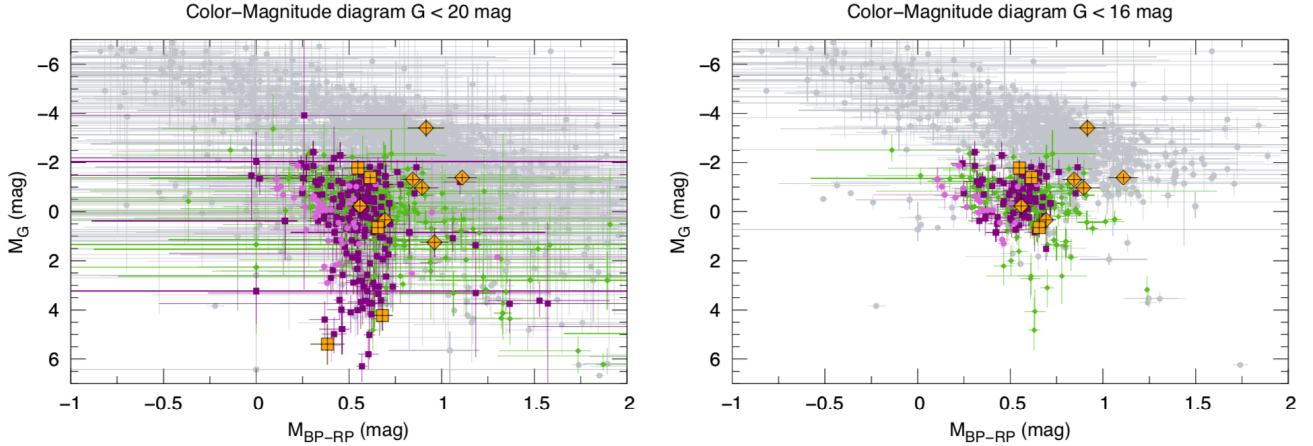


**Figure 10.** Color-magnitude diagrams for Cepheids with brightness limits of apparent magnitudes of 20 mag (left) and 16 mag (right) in Gaia *G* band. Absolute brightness values were computed based on distances by Bailer-Jones et al. (2018) considering interstellar dust. T2Cs (green) fundamental mode ACs (purple), overtone mode ACs (pink) and DCEPs (grey) were adopted from the catalogue by Ripepi et al. (2019) and Soszyński et al. (2017b, 2020a). *K2* targets are marked with large orange symbols.

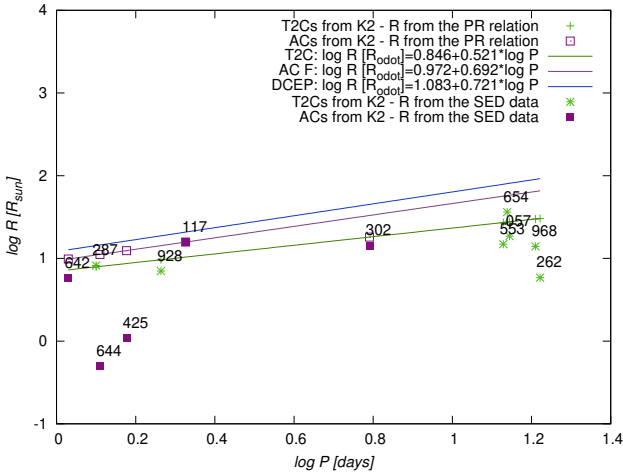


**Figure 11.** The period-radius relations for *K2* T2Cs and ACs, with the used relations. The blue PR-relation is for the DCEP-F from Groenewegen (2020):  $\log R = (0.721 \pm 0.013) \log P + (1.083 \pm 0.012)$ .

*Kepler* and *K2* missions is provided by the NASA Science Mission directorate.

Some of the data presented in this paper were obtained from the Mikulski Archive for Space Telescopes (MAST). STScI is operated by the Association of Universities for Research in Astronomy, Inc., under NASA contract NAS5-26555. Support for MAST for non-HST data is provided by the NASA Office of Space Science via grant NNX13AC07G and by other grants and contracts.

This work has made use of data from the European Space Agency (ESA) mission *Gaia* (<https://www.cosmos.esa.int/gaia>), processed by the *Gaia* Data Processing and Analysis Consortium (DPAC, <https://www.cosmos.esa.int/web/gaia/dpac/consortium>). Funding for the DPAC has been provided by national institutions, in particular the institutions participating in the *Gaia* Multilateral Agreement. This publication makes

use of data products from the Two Micron All Sky Survey, which is a joint project of the University of Massachusetts and the Infrared Processing and Analysis Center/California Institute of Technology, funded by the National Aeronautics and Space Administration and the National Science Foundation.

The DENIS project has been partly funded by the SCIENCE and the HCM plans of the European Commission under grants CT920791 and CT940627. It is supported by INSU, MEN and CNRS in France, by the State of Baden-Württemberg in Germany, by DGICYT in Spain, by CNR in Italy, by FFwFBWF in Austria, by FAPESP in Brazil, by OTKA grants F-4239 and F-013990 in Hungary, and by the ESO C&EE grant A-04-046.

Jean Claude Renault from IAP was the Project manager. Observations were carried out thanks to the contribution of numerous students and young scientists from all involved institutes, under the supervision of P. Fouqué, survey astronomer resident in Chile.

This publication makes use of data products from the Wide-field Infrared Survey Explorer, which is a joint project of the University of California, Los Angeles, and the Jet Propulsion Laboratory/California Institute of Technology, funded by the National Aeronautics and Space Administration. This work has made use of BaSTI web tools.

This project has been supported by the LP2012-31, LP2014-17, and LP2018-7 Lendület Programs of the Hungarian Academy of Sciences. MIJ acknowledges financial support from the Ministry of Education, Science and Technological Development of the Republic of Serbia through the contract number 451-03-68/2022-14/200002. This research was funded by DOMUS Grants of the Hungarian Academy of Sciences. Research was also supported by the Délvidékért Kiss Foundation, and the KKP-137523 ‘SeismoLab’ Élvonal grant of the Hungarian Research, Development and Innovation Office (NKFIH). This work is supported by the ERC via CoG-2016 RADIOSTAR (Grant Agreement 724560) and from work within the ‘ChETEC’ (CA16117), and the ‘MW-Gaia’ (CA18104) COST Actions funded by the COST program (European Cooperation in Science and Technology).

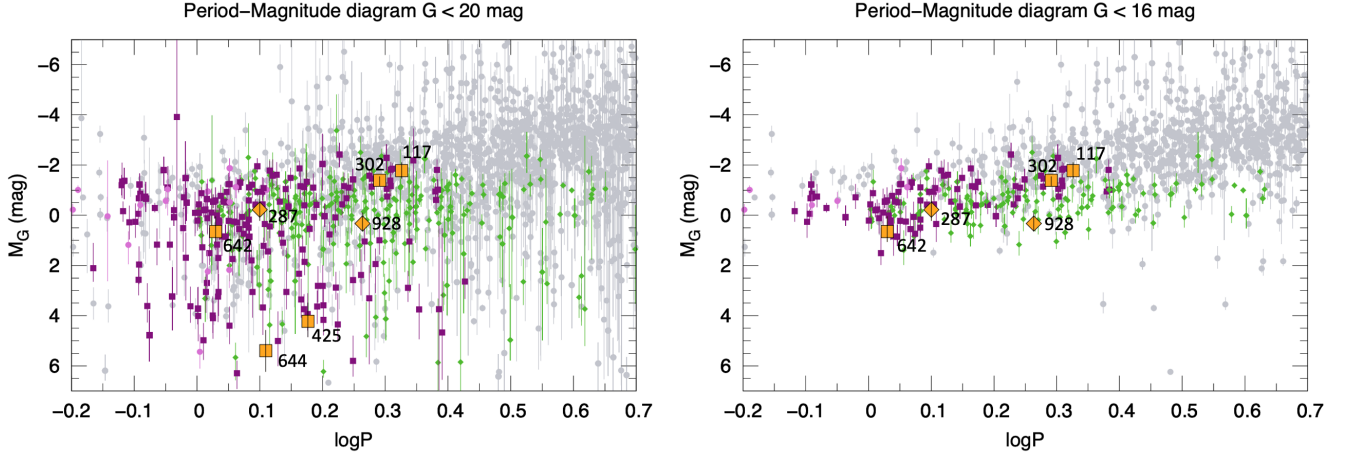


**Figure 12.** Period-magnitude diagrams for Cepheids with apparent brightness limit of 20 mag (left) and 16 mag (right) in Gaia  $G$  band. Absolute brightness values were computed based on distances by (Bailer-Jones et al. 2018) considering interstellar dust from the *Gaia* data base. The symbols are the same as in Figure 10.

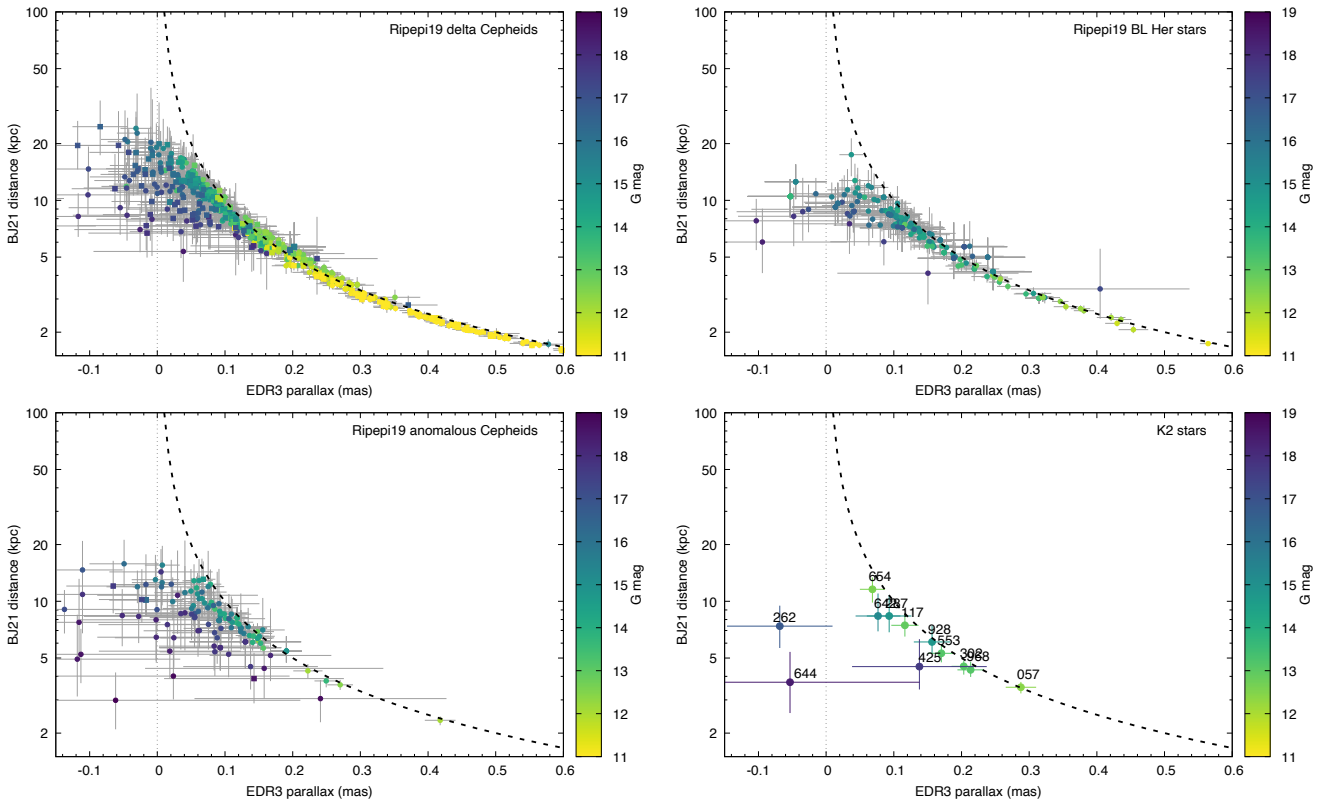


**Figure 13.** Gaia EDR3 parallaxes and geometric distances computed by Bailer-Jones et al. (2021) compared to each other. The black dashed line represents the simple  $d = 1/\pi$  inversion law. These plots clearly show that the calculated distances do not exceed 25 kpc, even for stars with very low parallaxes. For those stars the galactic model prior dominates the calculated distance, and it either underestimates the true distances for these stars or provides results that cannot be verified from the measured parallax.

## DATA AVAILABILITY

The Fourier decomposition data underlying this article are available in the article and in its online supplementary material. The photom-

etry data underlying this article will be shared on reasonable request by the corresponding author.

## REFERENCES

- Aigrain S., Parviainen H., Pope B. J. S., 2016, *MNRAS*, 459, 2408
- Anders F., et al., 2019, *A&A*, 628, A94
- Anders F., et al., 2022, *A&A*, 658, A91
- Astropy Collaboration et al., 2013, *A&A*, 558, A33
- Astropy Collaboration et al., 2018, *AJ*, 156, 123
- Baglin A., Auvergne M., Barge P., Michel E., Catala C., Deleuil M., Weiss W., 2007, in Dumitrache C., Popescu N. A., Suran M. D., Mioc V., eds, *American Institute of Physics Conference Series Vol. 895, Fifty Years of Romanian Astrophysics*. pp 201–209, doi:10.1063/1.2720423
- Bai Y., Liu J., Bai Z., Wang S., Fan D., 2019, *AJ*, 158, 93
- Bailer-Jones C. A. L., Rybizki J., Fouesneau M., Mantelet G., Andrae R., 2018, *AJ*, 156, 58
- Bailer-Jones C. A. L., Rybizki J., Fouesneau M., Demleitner M., Andrae R., 2021, *AJ*, 161, 147
- Benkő J. M., Szabó R., Dérkas A., Sódor Á., 2016, *MNRAS*, 463, 1769
- Berdnikov L. N., Pastukhova E. N., 2008, *Peremennye Zvezdy*, 28, 9
- Bhardwaj A., 2020, *Journal of Astrophysics and Astronomy*, 41, 23
- Bhardwaj A., Macri L. M., Rejkuba M., Kanbur S. M., Ngeow C.-C., Singh H. P., 2017, *AJ*, 153, 154
- Bhardwaj A., Braga V. F., Minniti D., Contreras Ramos R., Rejkuba M., 2021, in Kinemuchi K., Lovekin C., Neilson H., Vivas K., eds, *Astronomical Society of the Pacific Conference Series Vol. 529, RR Lyrae/Cepheid 2019: Frontiers of Classical Pulsators*. p. 259 (arXiv:2006.11855)
- Bianchi L., Shiao B., Thilker D., 2017, *ApJS*, 230, 24
- Bódi A., Szatmáry K., Kiss L. L., 2016, *A&A*, 596, A24
- Bódi A., Szabó P., Plachy E., Molnár L., Szabó R., 2021, arXiv e-prints, p. arXiv:2112.07496
- Bonifacio P., et al., 2021, *A&A*, 651, A79
- Bono G., et al., 2020, *A&A*, 644, A96
- Borucki W. J., 2016, *Reports on Progress in Physics*, 79, 036901
- Borucki W. J., et al., 2010, *Science*, 327, 977
- Braga V. F., et al., 2020, *A&A*, 644, A95
- Breger M., et al., 1993, *A&A*, 271, 482
- Buchler J. R., Moskalik P., 1992, *ApJ*, 391, 736
- Buder S., et al., 2021, *MNRAS*, 506, 150
- Caputo F., Castellani V., Degl’Innocenti S., Fiorentino G., Marconi M., 2004, *A&A*, 424, 927
- Catelan M., Smith H. A., 2015, *Pulsating Stars*. Wiley-VCH Verlag GmbH & Co. KGaA
- Cutri R. M., et al., 2003, *VizieR Online Data Catalog*, p. II/246
- Das S., Kanbur S. M., Smolec R., Bhardwaj A., Singh H. P., Rejkuba M., 2021, *MNRAS*, 501, 875
- Deacon N. R., Schlieder J. E., Olofsson J., Johnston K. G., Henning T., 2013, *MNRAS*, 434, 1117
- Drake A. J., et al., 2013, *ApJ*, 763, 32
- Drake A. J., et al., 2014, *ApJS*, 213, 9
- Epchtein N., et al., 1999, *A&A*, 349, 236
- Evans N. R., et al., 2015, *MNRAS*, 446, 4008
- Fiorentino G., Monelli M., 2012, *A&A*, 540, A102
- Fiorentino G., Limongi M., Caputo F., Marconi M., 2006, *A&A*, 460, 155
- Gaia Collaboration 2020, *VizieR Online Data Catalog*, p. I/350
- Gaia Collaboration et al., 2016, *A&A*, 595, A1
- Gaia Collaboration et al., 2018, *A&A*, 616, A1
- Gaia Collaboration et al., 2021, *A&A*, 649, A1
- Galicher R., et al., 2016, *A&A*, 594, A63
- Gautschi A., Saio H., 2017, *MNRAS*, 468, 4419
- Green G. M., Schlafly E., Zucker C., Speagle J. S., Finkbeiner D., 2019, *ApJ*, 887, 93
- Groenewegen M. A. T., 2012, *A&A*, 543, A36
- Groenewegen M. A. T., 2020, *A&A*, 635, A33
- Groenewegen M. A. T., Jurkovic M. I., 2017a, *A&A*, 603, A70
- Groenewegen M. A. T., Jurkovic M. I., 2017b, *A&A*, 604, A29
- Gustafsson B., Edvardsson B., Eriksson K., Jørgensen U. G., Nordlund Å., Plez B., 2008, *A&A*, 486, 951
- Hambálek L., Vaňko M., Panzen E., Smalley B., 2019, *MNRAS*, 483, 1642
- Hardegree-Ullman K. K., Zink J. K., Christiansen J. L., Dressing C. D., Ciardi D. R., Schlieder J. E., 2020, *ApJS*, 247, 28
- Hartman J. D., Bakos G. Á., Kovács G., Noyes R. W., 2010, *MNRAS*, 408, 475
- Henden A. A., 1980, *MNRAS*, 192, 621
- Herbst W., Shevchenko V. S., 1999, *AJ*, 118, 1043
- Hidalgo S. L., et al., 2018, *ApJ*, 856, 125
- Høg E., et al., 2000, *A&A*, 355, L27
- Howell S. B., et al., 2014, *PASP*, 126, 398
- Huber D., et al., 2016, *ApJS*, 224, 2
- Ivezic Z., Nenkova M., Elitzur M., 1999, *DUSTY: Radiation transport in a dusty environment* (ascl:9911.001)
- Jayasinghe T., et al., 2018, *MNRAS*, 477, 3145
- Jayasinghe T., et al., 2019a, *MNRAS*, 486, 1907
- Jayasinghe T., et al., 2019b, *Monthly Notices of the Royal Astronomical Society*, 491, 13
- Jurkovic M. I., 2018, *Serbian Astronomical Journal*, 197, 13
- Kiraga M., 2012, *Acta Astron.*, 62, 67
- Kochanek C. S., et al., 2017, *PASP*, 129, 104502
- Kovács G., Buchler J. R., 1988, *ApJ*, 334, 971
- Kovtyukh V., et al., 2018, *PASP*, 130, 054201
- Kwee K. K., Diethelm R., 1984, *A&AS*, 55, 77
- Lallement R., et al., 2018, *A&A*, 616, A132
- Lindgren L., et al., 2021, *A&A*, 649, A4
- Lomb N. R., 1976, *Ap&SS*, 39, 447
- Lucas P. W., et al., 2008, *MNRAS*, 391, 136
- Lucey M., Ting Y.-S., Ramachandra N. S., Hawkins K., 2020, *MNRAS*, 495, 3087
- Luo A. L., Zhao Y. H., Zhao G., et al. 2018, *VizieR Online Data Catalog*, p. V/153
- Manick R., et al., 2019, *A&A*, 628, A40
- Masters K. L., et al., 2010, *MNRAS*, 405, 783
- Matsunaga N., Feast M. W., Soszyński I., 2011, *MNRAS*, 413, 223
- McMahon R. G., Banerji M., Gonzalez E., Koposov S. E., Bejar V. J., Lodieu N., Rebolo R., VHS Collaboration 2013, *The Messenger*, 154, 35
- Miller A. A., 2015, *ApJ*, 811, 30
- Molnár L., et al., 2021, arXiv e-prints, p. arXiv:2109.07329
- Moskalik P., Buchler J. R., 1990, *ApJ*, 355, 590
- Moskalik P., Buchler J. R., 1993, *ApJ*, 406, 190
- Oláh K., et al., 2018, *A&A*, 620, A189
- Pecaut M. J., Mamajek E. E., 2016, *MNRAS*, 461, 794
- Percy J. R., 2007, *Understanding Variable Stars*. Cambridge : Cambridge University Press
- Plachy E., Molnár L., Jurkovic M. I., Smolec R., Moskalik P. A., Pál A., Szabados L., Szabó R., 2017, *MNRAS*, 465, 173
- Plachy E., Bódi A., Kolláth Z., 2018, *MNRAS*, 481, 2986
- Plachy E., et al., 2019, *ApJS*, 244, 32
- Plachy E., et al., 2021a, *ApJS*, 253, 11
- Plachy E., Szabó P., Bódi A., Molnár L., Szabó R., 2021b, in Kinemuchi K., Lovekin C., Neilson H., Vivas K., eds, *Astronomical Society of the Pacific Conference Series Vol. 529, Astronomical Society of the Pacific Conference Series*. p. 338 (arXiv:2009.08786)
- Pojmanski G., 1997, *Acta Astron.*, 47, 467
- Pojmanski G., 2002, *Acta Astron.*, 52, 397
- Poretti E., Le Borgne J. F., Rainer M., Baglin A., Benkő J. M., Debosscher J., Weiss W. W., 2015, *MNRAS*, 454, 849
- Rebull L. M., Stauffer J. R., Cody A. M., Hillenbrand L. A., David T. J., Pinsonneault M., 2018, *AJ*, 155, 196
- Ripepi V., Molinaro R., Musella I., Marconi M., Leccia S., Eyer L., 2019, *A&A*, 625, A14
- Samus’ N. N., et al., 2003, *Astronomy Letters*, 29, 468
- Samus’ N. N., Kazarovets E. V., Durlevich O. V., Kireeva N. N., Pastukhova E. N., 2017, *Astronomy Reports*, 61, 80
- Scargle J. D., 1982, *ApJ*, 263, 835
- Schmidt E. G., Hemen B., Rogalla D., Thacker-Lynn L., 2009, *AJ*, 137, 4598
- Schmidt E. G., Rogalla D., Thacker-Lynn L., 2011, *AJ*, 141, 53
- Simon N. R., 1986, *ApJ*, 311, 305
- Simon N. R., Lee A. S., 1981, *ApJ*, 248, 291



- Skrutskie M. F., et al., 2006, *AJ*, 131, 1163  
 Smolec R., 2016, *MNRAS*, 456, 3475  
 Smolec R., Moskalik P., 2012, *MNRAS*, 426, 108  
 Smolec R., Moskalik P., 2014, *MNRAS*, 441, 101  
 Smolec R., et al., 2012, *MNRAS*, 419, 2407  
 Smolec R., Moskalik P., Plachy E., Soszyński I., Udalski A., 2018, *MNRAS*, 481, 3724  
 Soszyński I., et al., 2008, *Acta Astron.*, 58, 293  
 Soszyński I., et al., 2011, *Acta Astron.*, 61, 285  
 Soszyński I., et al., 2015, *Acta Astron.*, 65, 233  
 Soszyński I., et al., 2017a, preprint, (arXiv:1712.01307)  
 Soszyński I., et al., 2017b, *Acta Astron.*, 67, 103  
 Soszyński I., Smolec R., Udalski A., Pietrukowicz P., 2019, *ApJ*, 873, 43  
 Soszyński I., et al., 2020a, *Acta Astron.*, 70, 101  
 Soszyński I., et al., 2020b, *ApJ*, 901, L25  
 Stassun K. G., Corsaro E., Pepper J. A., Gaudi B. S., 2018, *AJ*, 155, 22  
 Stassun K. G., et al., 2019, *AJ*, 158, 138  
 Stetson P. B., Fiorentino G., Bono G., Bernard E. J., Monelli M., Iannicola G., Gallart C., Ferraro L., 2014, *PASP*, 126, 616  
 Stevens D. J., Stassun K. G., Gaudi B. S., 2017, *AJ*, 154, 259  
 Tonry J. L., et al., 2018, *ApJ*, 867, 105  
 Udalski A., Szymański M. K., Szymański G., 2015, *Acta Astron.*, 65, 1  
 Uitterdijk J., 1935, *Bull. Astron. Inst. Netherlands*, 7, 304  
 Vega L. D., Stassun K. G., Montez Rodolfo J., Boyd P. T., Somers G., 2017, *ApJ*, 839, 48  
 Vida K., Plachy E., Molnar L., Kriskovics L., Klagyivik P., Hajdu T., Kovacs O. E., Szabo R., 2016, *Information Bulletin on Variable Stars*, 6173, 1  
 Virtanen P., et al., 2020, *Nature Methods*, 17, 261  
 Wielgórski P., et al., 2022, *ApJ*, 927, 89  
 Wright E. L., et al., 2010, *AJ*, 140, 1868  
 Xiang M., et al., 2019, *ApJS*, 245, 34  
 Zejda M., Paunzen E., Baumann B., Mikulášek Z., Liška J., 2012, *A&A*, 548, A97

#### APPENDIX A: FOURIER PARAMETERS CALCULATED FROM OGLE V BAND MEASUREMENTS FOR LMC CEPHEIDS

The Fourier parameters for the pulsating stars from the OGLE V band catalog were calculated using the same method as described in Section 2, so that our comparison on the Fourier parameter plots would be as calculated in a consistent manner. The calculated Fourier parameters are given in the Table A1 in a short format and are available fully online.

#### APPENDIX B: RV TAURI STARS

In the K2 proposals two RV Tauri stars were observed as shown in Table B1. The time span of observations in a given Campaign (less than 90 days) limits the scientific value of these long-period stars. These observations will be useful when additional data will be collected, so these data can contribute to the understanding of the pulsation of RV Tauri stars. The star EPIC 212146366 was observed in Campaigns 5 (two consecutive pulsational periods were covered) and 18. In case of EPIC 249577490 in Campaign 15 four pulsation periods were measured.

#### APPENDIX C: NON T2C AND AC STARS

The original TESS Asteroseismic Science Collaboration proposals for the K2 observing campaigns contained lists of pulsating stars that were collected from the literature. Table C1 shows the list of stars

that were among the observed stars, but after closer examination turned out not to be T2Cs or ACs. The light curves of these stars are quite diverse. In some cases we have determined that the variable in question is a DCEP (see 210426515, 211394018 and 247086981). There are two RRL type variable stars: 246395799 and 247520086. Some are changing their light curve due to being rotating spotted stars, ellipsoidal variables, eclipsing binaries. The star 246104577 is a triple star system with a debris disk. Some stars show flares in their light curve. Flares are not possible on T2Cs, so we have excluded them from the final list. Many of the observed stars are young stars (T Tauri type). There is a semi regular (SR), an irregular (L) and a RS CVn type variable as well. For the long period variable stars, typically 1.5-2.0 cycles of variation were observed in one campaign.

This paper has been typeset from a  $\text{\LaTeX}$  file prepared by the author.

**Table A1.** Fourier parameters calculated from OGLE V band measurements for LMC Cepheids

Name	Type	Period (d)	$R_{21}$	$\sigma R_{21}$	$\phi_{21}$	$\sigma \phi_{21}$	$R_{31}$	$\sigma R_{31}$	$\phi_{31}$	$\sigma \phi_{31}$
OGLE-LMC-CEP-0002	DCEP-F	3.118121	0.314	0.005	4.238	0.051	0.117	0.005	2.283	0.083
OGLE-LMC-CEP-0012	DCEP-F	2.660176	0.460	0.003	3.984	0.024	0.290	0.002	2.032	0.036
OGLE-LMC-CEP-0017	DCEP-F	3.677228	0.481	0.003	4.337	0.024	0.283	0.003	2.420	0.037
OGLE-LMC-CEP-0023	DCEP-F	1.701824	0.478	0.006	3.780	0.046	0.163	0.005	1.820	0.072
OGLE-LMC-CEP-0025	DCEP-F	3.733530	0.417	0.004	4.236	0.043	0.153	0.004	2.319	0.069
OGLE-LMC-CEP-0026	DCEP-F	2.570668	0.455	0.003	4.057	0.016	0.234	0.002	1.961	0.025
OGLE-LMC-CEP-0027	DCEP-F	3.522950	0.435	0.002	4.213	0.017	0.243	0.002	2.085	0.025
OGLE-LMC-CEP-0028	DCEP-F	1.262950	0.468	0.004	3.770	0.035	0.299	0.005	1.552	0.051
OGLE-LMC-CEP-0037	DCEP-F	3.066901	0.372	0.005	4.057	0.054	0.096	0.005	2.142	0.088
OGLE-LMC-CEP-0039	DCEP-F	3.147752	0.403	0.004	4.246	0.041	0.203	0.004	2.261	0.065
...										

**Table B1.** Type II Cepheids with long periods, which means that the cycle coverage was not enough for a detailed analysis of the pulsation. Reference <sup>1</sup>: SIMBAD Astronomical Database (<http://simbad.u-strasbg.fr/simbad/>)

C.	EPIC ID	RA [h m s]	DEC [° ' "]	Remark	Source
5, 18	212146366	08 26 10.154	+22 57 17.81	Redder T2C	Schmidt et al. (2009) (wrong period)
15	249577490	15 42 00.050	-20 46 45.92	RX Lib–RV Tau	SIMBAD <sup>1</sup>

**Table C1.** Stars that were found to be classical Cepheids (DCEP), Cepheid variable stars (CEP), RR Lyrae variable stars (RRab and RRC), semi-regular variables (SR, SRD), BY Dra type variable stars (BY Dra), T Tauri type variables (T Tauri), young stellar objects (YSO), irregular variables (L), spotted stars, rotational variables (ROT), eclipsing binaries (EC), binary or triple stars, and others. These stars were observed in the examined Campaigns, and had light curves that could have resemble Type II Cepheids or anomalous Cepheids.

C.	EPIC ID	RA [h m s]	DEC [° ' "]	Remark	Source
2	202571062	16 24 02.038	-29 10 44.82	Pre-main sequence EB	Vida et al. (2016)
2	204121113	16 09 58.630	-23 34 55.91	ROT	Rebull et al. (2018)
2	204264833	16 23 07.782	-23 00 59.58	T Tauri	Pecaut & Mamajek (2016)
2	204894575	16 02 53.963	-20 22 48.00	T Tauri	Pecaut & Mamajek (2016)
2	205023358	15 55 06.701	-19 46 31.33	ROT or BY Dra	Kiraga (2012) or Samus' et al. (2003)
3	205964079	22 24 45.925	-15 54 48.32	Spotted flare star	This article
4	210990639	04 11 08.549	+22 49 31.31	Binary (eclipse seen)	This article
4	210426515	03 49 17.915	+14 03 14.59	ROT:	ASAS-SN (Kochanek et al. 2017)
4	210525462	04 05 26.387	+15 49 49.88	L	ASAS-SN (Jayasinghe et al. 2018)
4	210708282	03 28 08.580	+18 28 54.71	ROT or EC/CW-FO/ESD	Hartman et al. (2010) or Pojmanski (2002)
4	210785321	03 28 13.447	+19 38 44.96	L	ASAS-SN (Jayasinghe et al. 2019a)
4	210800332	04 02 59.906	+19 52 20.76	MISC/CW	Pojmanski (2002)
5	211394018	08 35 22.466	+11 32 57.93	DCEP	Schmidt et al. (2011)
5, 18	211584699	08 12 49.000	+14 19 52.89	L	ASAS-SN Jayasinghe et al. (2019a)
5	211759736	08 15 12.967	+16 44 41.47	Spotted giant star in an EC	Oláh et al. (2018)
7	214047277	18 56 17.534	-27 31 25.62	V4061 Sgr-SRD	ASAS-SN (Jayasinghe et al. 2019a)
7	217257168	18 57 51.984	-20 53 37.05	SR	Samus' et al. (2017)
7	218177215	18 56 25.238	-19 16 22.87	Dwarf nova	This article
10	201419619	12 07 56.712	-00 39 37.62	Binary star	This article
10	228811074	12 28 12.493	-06 19 00.53	ROT with flares	This article
12, 19	246104577	22 59 34.998	-07 02 22.87	Triple system with debris disk	Deacon et al. (2013)
12	246263296	23 36 06.012	-03 47 47.82	ROT with spots and flares	This article, ROT-ASAS-SN (Jayasinghe et al. 2019b)
12	246395799	23 13 55.646	-01 07 25.08	RRc	This article
13	210670948	04 32 09.287	+17 57 22.69	Weak T Tauri	Herbst & Shevchenko (1999)
13	210698281	04 32 14.568	+18 20 14.84	Weak T Tauri	Herbst & Shevchenko (1999)
13	246736776	05 01 29.240	+15 01 26.35	ROT	ASAS-SN (Jayasinghe et al. 2019a)
13	246773415	05 00 49.288	+15 27 00.72	YSO	Galicher et al. (2016)
13	246782263	04 32 56.252	+15 32 53.20	Spotted, flare star with eclipses	This article
13	247086981	04 37 14.779	+18 32 34.92	SZ Tau-DCEP	Evans et al. (2015)
13	247454835	04 31 16.860	+21 50 25.26	T Tau type	Hambálek et al. (2019)
13	247520086	04 58 08.497	+22 20 59.86	RRab	Drake et al. (2013)
13	247671949	04 57 47.113	+23 30 26.25	ROT:	ASAS-SN (Jayasinghe et al. 2019a)
15	249104247	15 22 16.298	-26 52 25.54	RS CVn (X-ray source)	PX Lib Berdnikov & Pastukhova (2008)
15	249483655	15 26 02.036	-21 56 36.24	Eclipsing ellipsoidal binary	This article ROT-ASAS-SN (Jayasinghe et al. 2019a)
15	249926841	15 30 48.035	-16 19 23.04	Spotted, flare star	This article, ROT-ASAS-SN (Jayasinghe et al. 2019a)
15	250178428	15 29 43.29	-13 10 52.00	YSO	ASAS-SN (Jayasinghe et al. 2019a)
19	251737903	22 55 18.04	+01 11 53.62	Galaxy	Masters et al. (2010)